



HAL
open science

Novel Copper Complexes as Visible Light Photoinitiators for the Synthesis of Interpenetrating Polymer Networks (IPNs)

Mahmoud Rahal, Guillaume Noirbent, Bernadette Graff, Joumana Toufaily,
Tayssir Hamieh, Didier Gignes, Frederic Dumur, Jacques Lalevée

► **To cite this version:**

Mahmoud Rahal, Guillaume Noirbent, Bernadette Graff, Joumana Toufaily, Tayssir Hamieh, et al..
Novel Copper Complexes as Visible Light Photoinitiators for the Synthesis of Interpenetrating Polymer
Networks (IPNs). *Polymers*, 2022, 14 (10), pp.1998. 10.3390/polym14101998 . hal-03668117

HAL Id: hal-03668117

<https://hal.science/hal-03668117>

Submitted on 14 May 2022

HAL is a multi-disciplinary open access archive for the deposit and dissemination of scientific research documents, whether they are published or not. The documents may come from teaching and research institutions in France or abroad, or from public or private research centers.

L'archive ouverte pluridisciplinaire **HAL**, est destinée au dépôt et à la diffusion de documents scientifiques de niveau recherche, publiés ou non, émanant des établissements d'enseignement et de recherche français ou étrangers, des laboratoires publics ou privés.



Distributed under a Creative Commons Attribution 4.0 International License

Article

Novel Copper Complexes as Visible Light Photoinitiators for the Synthesis of Interpenetrating Polymer Networks (IPNs)

Mahmoud Rahal^{1,2,3}, Guillaume Noirbent⁴ , Bernadette Graff^{1,2}, Joumana Toufaily³ , Tayssir Hamieh³ ,
Didier Gigmes⁴, Frédéric Dumur^{4,*}  and Jacques Lalevée^{1,2,*} 

¹ Université de Haute-Alsace, CNRS, IS2M UMR 7361, F-68100 Mulhouse, France; mahmoud-rahall@outlook.com (M.R.); bernadette.graff@uha.fr (B.G.)

² Université de Strasbourg, F-67087 Strasbourg, France

³ Laboratory of Materials, Catalysis, Environment and Analytical Methods (MCEMA) and LEADDER Laboratory, Faculty of Sciences, Doctoral School of Sciences and Technology (EDST), Lebanese University, Beirut 6573-14, Lebanon; joumana.toufaily@ul.edu.lb (J.T.); tayssir.hamieh@ul.edu.lb (T.H.)

⁴ Aix Marseille Univ, CNRS, ICR UMR 7273, F-13397 Marseille, France; guillaume.noirbent@outlook.fr (G.N.); didier.gigmes@univ-amu.fr (D.G.)

* Correspondence: frederic.dumur@univ-amu.fr (F.D.); jacques.lalevee@uha.fr (J.L.)

Abstract: This work is devoted to the study of two copper complexes (Cu) bearing pyridine ligands, which were synthesized, evaluated and tested as new visible light photoinitiators for the free radical photopolymerization (FRP) of acrylates functional groups in thick and thin samples upon light-emitting diodes (LED) at 405 and 455 nm irradiation. These latter wavelengths are considered to be safe to produce polymer materials. The photoinitiation abilities of these organometallic compounds were evaluated in combination with an iodonium (Iod) salt and/or amine (e.g., *N*-phenylglycine—NPG). Interestingly, high final conversions and high polymerization rates were obtained for both compounds using two and three-component photoinitiating systems (Cu1 (or Cu2)/Iodonium salt (Iod) (0.1%/1% *w/w*) and Cu1 (or Cu2)/Iod/amine (0.1%/1%/1% *w/w/w*). The new proposed copper complexes were also used for direct laser write experiments involving a laser diode at 405 nm, and for the photocomposite synthesis with glass fibers using a UV-conveyor at 395 nm. To explain the obtained polymerization results, different methods and characterization techniques were used: steady-state photolysis, real-time Fourier transform infrared spectroscopy (RT-FTIR), emission spectroscopy and cyclic voltammetry.

Keywords: copper complex; photocomposite; LED; laser write; free radical photopolymerization



Citation: Rahal, M.; Noirbent, G.; Graff, B.; Toufaily, J.; Hamieh, T.; Gigmes, D.; Dumur, F.; Lalevée, J. Novel Copper Complexes as Visible Light Photoinitiators for the Synthesis of Interpenetrating Polymer Networks (IPNs). *Polymers* **2022**, *14*, 1998. <https://doi.org/10.3390/polym14101998>

Academic Editor: Houwen Matthew Pan

Received: 22 April 2022

Accepted: 9 May 2022

Published: 13 May 2022

Publisher's Note: MDPI stays neutral with regard to jurisdictional claims in published maps and institutional affiliations.



Copyright: © 2022 by the authors. Licensee MDPI, Basel, Switzerland. This article is an open access article distributed under the terms and conditions of the Creative Commons Attribution (CC BY) license (<https://creativecommons.org/licenses/by/4.0/>).

1. Introduction

The elaboration of polymers by photochemical means, such as free radical photopolymerization (FRP) and cationic photopolymerization (CP), have been mainly based on the use of metal-free organic dyes and photoinitiators at the industrial and academic levels [1–12], and these synthetic processes (FRP and CP) are widely used in different fields, e.g., dentistry [13–23], adhesives [24–28], coatings [29–33], composites [34], medicine [35–40], direct laser write, 3D and 4D printing [41–50], etc. On the other hand, organometallic compounds are not really used in industry; in other words, manufacturers avoid incorporating metallic compounds in their synthetic formulations due to their potential toxicity and price [51–64]. With their photochemical properties, such as high-absorption properties in the near-UV and visible range [65–68], long-lived excited states [69–74], suitable redox potentials [75–89], copper complexes can be used as photoinitiators (PIs)/photoredox catalysts able to produce active species, according to a catalytic cycle [90,91]. Therefore, it is very important to develop new metal-free photoinitiators or low-cost organometallic-based complexes [92–95].

In fact, copper complexes have attracted much attention and intense efforts have been devoted in recent years to the development of new copper complexes of improved

photosensitivity, due to their competitive costs compared to other metal complexes. Copper complexes bearing a pyridine-based chelate ligand showed excellent photochemical properties for photocatalysis process, such as high-oxidation potential in the excited state [96–99], long-excited-state lifetime, high-emission quantum yields and high-absorption properties in the UV-visible region. Furthermore, copper complex derivatives have already been tested as PIs for FRP, CP, as well as IPN synthesis [100–104].

In this paper, two new copper complexes (Cu1–Cu2) (Figure 1) were synthesized and investigated as visible light photoinitiators upon exposure to LEDs at 405 and 455 nm for FRP, CP and the synthesis of interpenetrating polymer networks (IPNs) of acrylate/epoxy monomer blends. These compounds will be incorporated in two (Cu1 (or Cu2)/Iod (0.1%/1% *w/w*)) and three-component (Cu1 (or Cu2)/Iod/NPG (0.1%/1%/1% *w/w/w*)) photoinitiating systems (PISs) to produce polymer materials by free radical photopolymerization and the polymerization of acrylate/epoxy blend (IPNs). The photoinitiating ability of copper complexes will also be explained based on the interaction of Cu1 (or Cu2)/Iod and Cu1 (or Cu2)/Iod/NPG, which can be studied using different techniques and characterization processes, e.g., steady-state photolysis, cyclic voltammetry, fluorescence quenching and electron spin resonance spin trapping. Finally, to demonstrate the effectiveness of these new copper complex-based photoinitiators, experiments using direct laser writing (DLW), 3D printing and photocomposites synthesis were carried out in this work using different irradiation sources.

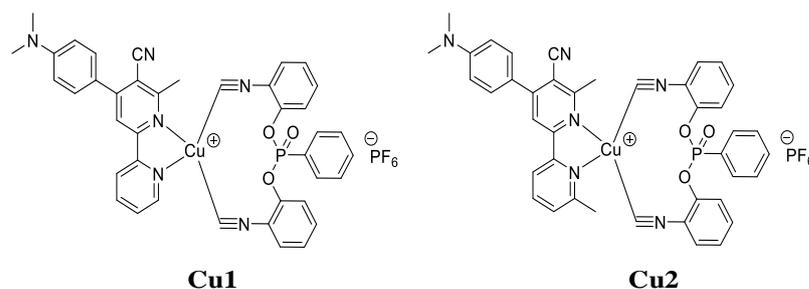


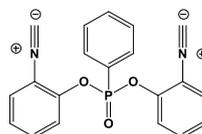
Figure 1. Copper complexes used in this work as PIs.

2. Materials and Methods

2.1. Synthesis of Chalcones, Ligands and Copper Complexes

Experimental conditions and acquisition conditions have been detailed elsewhere [13,92,100]. The two chalcones used for the design of ligands L1 and L2 were then engaged in a cyclization reaction with β -aminocrotonitrile according to a reaction reported in 1992 by Masaki Matsui [105,106]. *Bis*(2-isocyanophenyl) phenylphosphonate (binc) was synthesized by adapting a literature procedure [107,108].

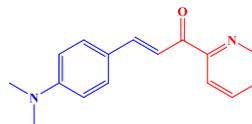
Synthesis of bis(2-isocyanophenyl) phenylphosphonate (binc)



Benzoxazole (9.1 g, 76.3 mmol, 1.0 equiv.) was dissolved in dry THF (200 mL). The solution was cooled at $-78\text{ }^{\circ}\text{C}$ and *n*-BuLi (2.5 M in hexane, 32.0 mL, 80.0 mmol, 1.05 equiv.) was added. Stirring was maintained for 1.5 h at this temperature. Phenyl phosphonic dichloride (5.7 mL, 4.04 mmol, 0.53 equiv.) was added and the solution could warm to room temperature. The solution was poured in $\text{Et}_2\text{O}:\text{NaHCO}_3$ (2:1, 150 mL). The organic phase was washed with water several times, dried over magnesium sulfate and the solvent removed under reduced pressure. The residue was crystallized in pentane/ethyl acetate (4/1) to provide the ligand (55% yield) as a light brown solid. ^1H NMR (400 MHz, CDCl_3) δ (ppm): 8.23–8.11 (m, 2H), 7.69 (td, $J = 7.4, 1.3$ Hz, 1H), 7.58 (dt, $J = 12.5, 6.3$ Hz, 2H), 7.48 (d, $J = 8.4$ Hz, 2H), 7.39 (d, $J = 7.9$ Hz, 2H), 7.34 (td, $J = 8.1, 1.6$ Hz, 2H), 7.18 (t, $J = 7.7$ Hz,

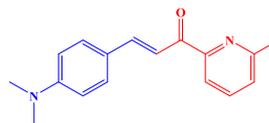
2H); ^{13}C NMR (101 MHz, CDCl_3) δ (ppm): 169.7, 145.7, 145.7, 134.5, 132.9, 132.8, 130.7, 130.7, 129.3, 129.1, 128.3, 125.9, 124.1, 124.1, 121.7, 121.7. (isonitrile carbons not detected); HRMS (ESI MS) m/z : theor: 360.0664 found: 360.0666 (M^+ detected).

Synthesis of (E)-3-(4-(dimethylamino)phenyl)-1-(pyridin-2-yl)prop-2-en-1-one



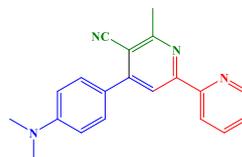
Next, 4-(Dimethylamino)benzaldehyde (1.49 g, 10.0 mmol, $M = 149.19$ g/mol) and 1-(pyridin-2-yl)ethan-1-one (1.21 g, 10.0 mmol, $M = 121.14$ g/mol) were suspended in ethanol (50 mL) and aq. KOH (40%) (10 mL) was added. After stirring overnight, the solid was filtered off, washed with ethanol and water, and dried under vacuum. The product was purified by filtration on a plug of SiO_2 using dichloromethane (DCM) as the eluent (2.32 g, 92% yield). ^1H NMR (400 MHz, CDCl_3) δ (ppm): 8.61–8.49 (m, 1H), 8.01 (d, $J = 7.4$ Hz, 1H), 7.92 (d, $J = 15.8$ Hz, 1H), 7.77 (d, $J = 15.8$ Hz, 1H), 7.66 (t, $J = 7.0$ Hz, 1H), 7.45 (d, $J = 7.7$ Hz, 2H), 7.31–7.22 (m, 1H), 6.49 (d, $J = 7.8$ Hz, 2H), 2.83 (s, 6H); ^{13}C NMR (101 MHz, CDCl_3) δ (ppm): 189.16, 155.00, 152.11, 148.69, 145.94, 136.89, 130.90, 126.40, 122.99, 122.72, 115.47, 111.74, 40.06; HRMS (ESI MS) m/z : theor: 253.1296 found: 253.1299 ($[\text{M} + \text{H}]^+$ detected).

Synthesis of (E)-3-(4-(dimethylamino)phenyl)-1-(6-methylpyridin-2-yl)prop-2-en-1-one



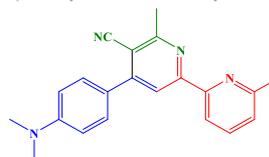
Following this, 4-(Dimethylamino)benzaldehyde (2.21 g, 14.8 mmol, $M = 149.19$ g/mol) and 1-(6-methylpyridin-2-yl)ethan-1-one (2.00 g, 14.8 mmol, $M = 135.17$ g/mol) were dissolved in ethanol (50 mL) and aq. KOH (40%) (15 mL) was added. After stirring the solution overnight, the resulting solid was filtered off. It was purified by filtration on a plug of SiO_2 using DCM as the eluent. For a higher purity, the solid was first dissolved in DCM and precipitated by addition of pentane (3.51 g, 89% yield). ^1H NMR (400 MHz, CDCl_3) δ (ppm): 8.02 (d, $J = 15.8$ Hz, 1H), 7.90 (d, $J = 7.5$ Hz, 1H), 7.84 (d, $J = 15.9$ Hz, 1H), 7.65 (t, $J = 7.7$ Hz, 1H), 7.58–7.53 (m, 2H), 7.23 (d, $J = 7.4$ Hz, 1H), 6.66–6.60 (m, 2H), 2.97 (s, 6H), 2.60 (s, 3H); ^{13}C NMR (101 MHz, CDCl_3) δ (ppm): 189.62, 157.67, 154.57, 152.04, 145.63, 136.95, 130.84, 126.02, 123.26, 119.84, 115.94, 111.77, 40.13, 24.54; HRMS (ESI MS) m/z : theor: 267.1453 found: 267.1451 ($[\text{M} + \text{H}]^+$ detected).

Synthesis of 4-(4-(dimethylamino)phenyl)-6-methyl-[2,2'-bipyridine]-5-carbonitrile



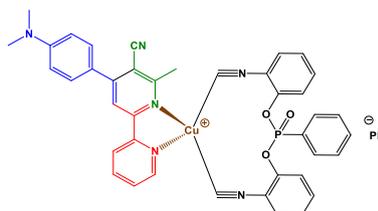
Potassium *tert*-butoxide (1.2 g) and β -aminocrotonitrile (4.92 g, 60 mmol, $M = 82.10$ g/mol) were dissolved in acetonitrile (300 mL) and the solution was heated at 35°C for 15 min. Chalcone (E)-3-(4-(dimethylamino)phenyl)-1-(pyridin-2-yl)prop-2-en-1-one (2.52 g, 10.0 mmol, $M = 252.32$ g/mol) was added and stirring was maintained for three days. The solid was filtered off and washed with ethanol and water. It was purified by filtration on a plug of SiO_2 using DCM as the eluent (2.83 g, 90% yield). ^1H NMR (400 MHz, CDCl_3) δ (ppm): 8.70 (ddd, $J = 4.8, 1.7, 0.9$ Hz, 1H), 8.50 (dt, $J = 8.0, 1.0$ Hz, 1H), 8.40 (s, 1H), 7.85 (td, $J = 7.8, 1.8$ Hz, 1H), 7.72–7.64 (m, 2H), 7.36 (ddd, $J = 7.5, 4.8, 1.2$ Hz, 1H), 6.85–6.77 (m, 2H), 3.05 (s, 6H), 2.89 (s, 3H); ^{13}C NMR (101 MHz, CDCl_3) δ (ppm): 162.47, 157.15, 155.03, 154.08, 151.47, 149.38, 137.02, 129.74, 129.74, 124.47, 123.44, 122.10, 118.22, 117.68, 111.97, 111.97, 106.10, 40.19, 40.19, 24.38; HRMS (ESI MS) m/z : theor: 315.1565 found: 315.1564 ($[\text{M} + \text{H}]^+$ detected).

Synthesis of 4-(4-(dimethylamino)phenyl)-6,6'-methyl-[2,2'-bipyridine]-5-carbonitrile



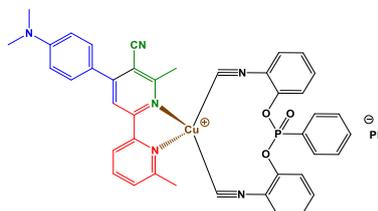
Potassium *tert*-butoxide (1.2 g) and β -aminocrotonitrile (4.92 g, 60 mmol, $M = 82.10$ g/mol) were dissolved in acetonitrile (300 mL) and the solution was heated at 35 °C for 15 min. Chalcone (*E*)-3-(4-(dimethylamino)phenyl)-1-(6-methylpyridin-2-yl)prop-2-en-1-one (L3) (2.66 g, 10.0 mmol, $M = 266.34$ g/mol) was added and stirring was maintained for three days. The solid was filtered off and washed with ethanol and water. It was purified by filtration on a plug of SiO₂ using DCM as the eluent (2.76 g, 84% yield). ¹H NMR (400 MHz, CDCl₃) δ (ppm): 8.40 (s, 1H), 8.27 (d, $J = 7.8$ Hz, 1H), 7.72 (t, $J = 7.8$ Hz, 1H), 7.69–7.63 (m, 2H), 7.21 (d, $J = 7.6$ Hz, 1H), 6.85–6.79 (m, 2H), 3.05 (s, 6H), 2.88 (s, 3H), 2.63 (s, 3H); ¹³C NMR (101 MHz, CDCl₃) δ (ppm): 162.36, 158.24, 157.56, 154.37, 154.00, 151.43, 137.13, 129.70, 129.70, 124.09, 123.68, 119.11, 118.27, 117.78, 112.01, 112.01, 105.95, 40.21, 40.21, 24.61, 24.38; HRMS (ESI MS) m/z : theor: 329.1722 found: 329.1719 ([$M + H$]⁺ detected).

Synthesis of Cu1



Tetrakis(acetonitrile)copper(I) hexafluorophosphate (372 mg, 1.0 mmol, $M = 372.72$ g/mol), *bis*(2-isocyanophenyl)phenylphosphonate (binc) (360 mg, 1.0 mmol, $M = 360.31$ g/mol) and 4-(4-(dimethylamino)phenyl)-6,6'-methyl-[2,2'-bipyridine]-5-carbonitrile (314 mg, 1.0 mmol, $M = 314.39$ g/mol) were dissolved in DCM (100 mL) and the solution was stirred at 25 °C for 2 h. The solution was concentrated to ca. 5 mL. Diethyl ether was added, as the product was a solid (866 mg, 98% yield). ¹H NMR (400 MHz, CDCl₃) δ (ppm): 8.96 (s, 1H), 8.51 (s, 1H), 8.26 (s, 1H), 8.14 (dd, $J = 14.2, 7.6$ Hz, 2H), 7.85–7.70 (m, 4H), 7.70–7.59 (m, 4H), 7.52–7.35 (m, 5H), 7.24 (t, $J = 8.1$ Hz, 2H), 6.94 (s (br), 2H), 3.21 (s, 3H), 3.11 (s, 6H); HRMS (ESI MS) m/z : theor: 737.1486 found: 737.1481 (M^+ detected); Anal. Calc. for C₄₀H₃₁CuF₆N₆O₃P₂: C, 54.4; H, 3.5; O, 5.4; Found: C, 54.6; H, 3.4; O, 5.5%.

Synthesis of Cu2



Tetrakis(acetonitrile)copper(I) hexafluorophosphate (372 mg, 1.0 mmol, $M = 372.72$ g/mol), *bis*(2-isocyanophenyl)phenyl phosphonate (binc) (360 mg, 1.0 mmol, $M = 360.31$ g/mol) and 4-(4-(dimethylamino)phenyl)-6,6'-methyl-[2,2'-bipyridine]-5-carbonitrile (328 mg, 1.0 mmol, $M = 328.42$ g/mol) were dissolved in DCM (100 mL) and the solution was stirred at 25 °C for 2 h. The solution was concentrated to ca. 5 mL. Addition of diethyl ether precipitated the product as a yellow solid (883 mg, 98% yield). ¹H NMR (400 MHz, DMSO) δ (ppm): 8.76 (s, 1H), 8.62 (s, 1H), 8.21 (s, 1H), 8.02 (dd, $J = 13.2, 7.2$ Hz, 2H), 7.79 (s, 6H), 7.67 (s, 2H), 7.56 (t, $J = 7.9$ Hz, 2H), 7.35 (dd, $J = 21.3, 8.0$ Hz, 5H), 6.92 (d, $J = 8.8$ Hz, 2H), 3.14 (s, 3H), 3.06 (s, 6H), 2.93 (s, 3H); HRMS (ESI MS) m/z : theor: 751.1642 found: 751.1639 (M^+ detected); Anal. Calc. for C₄₁H₃₃CuF₆N₆O₃P₂: C, 54.9; H, 3.7; O, 5.3; Found: C, 55.0; H, 3.4; O, 5.5%.

2.2. Other Chemicals

Chemical structure of the different monomers and additives are presented in Figure 2. Di-*tert*-butyl-diphenyl iodonium hexafluorophosphate (Iod) and ethyl 4-(dimethylamino)benzoate (EDB) were obtained from Lambson Ltd. (UK). Di(trimethylolpropane) tetraacrylate (TA), trimethylolpropane triacrylate (TMPTA), (3,4-epoxycyclohexane)methyl 3,4-epoxycyclohexylcarboxylate (EPOX; Uvacure 1500), *N*-phenylglycine (NPG), *N*-vinylcarbazole (NVK) and *N,N*-dimethyl-*p*-toluidine (TMA) were obtained from Allnex or Sigma Aldrich. TA, TMPTA and EPOX were chosen as acrylic and cationic monomers for the radical and cationic polymerizations.

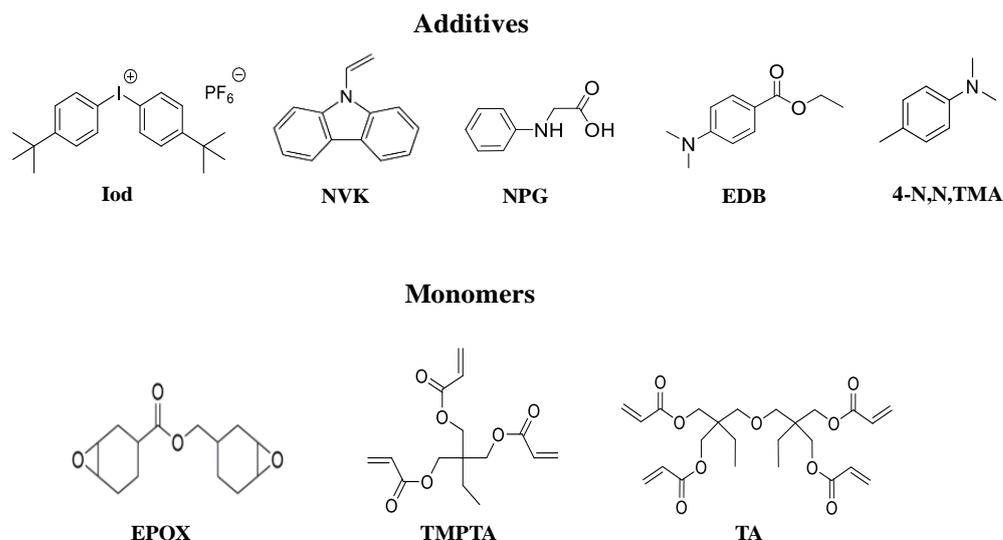


Figure 2. Other organic compounds used.

2.3. Irradiation Sources: Light-Emitting Diodes

All the irradiation sources used during these experiments are based on light-emitting diodes (LEDs) and used as safe sources: (1) LED at 375 nm ($I_0 = 75 \text{ mW} \cdot \text{cm}^{-2}$) for the photolysis experiments, (2) LED at 405 nm ($I_0 = 110 \text{ mW} \cdot \text{cm}^{-2}$) and 455 nm ($I_0 = 75 \text{ mW} \cdot \text{cm}^{-2}$) for the photopolymerization experiments, (3) LED conveyor at 395 nm ($I_0 = 4 \text{ W} \cdot \text{cm}^{-2}$) for the photocomposite synthesis.

2.4. Photopolymerization Kinetics Determination by Real-Time Fourier Transform Infrared Spectroscopy (RT-FTIR)

In the present work, copper derivatives were used in two and three-component PISs for both FRP and CP under irradiation with LEDs at 405 and 455 nm. PISs were mainly based on two-component Cu1 (or Cu2)/Iod (0.1%-0.2%-0.5%/1% *w/w*) and three-component Cu1 (or Cu2)/Iod/amine (NPG, NVK) (0.1%/1%/1% *w/w/w*) systems. The weight percent of the photoinitiating (PI, co-initiator and amine) system was calculated from the global monomer content. Firstly, two different samples were studied for each photosensitive formulation in (i) thick (thickness = 1.4 mm) and (ii) thin samples (thickness = 25 μm). The epoxy and acrylate conversions were continuously followed by RT-FTIR using a JASCO FTIR 6600 (JASCO France, Lisses, France), so it was possible to determine the final conversion of reactive functions and to calculate the polymerization rate of each kinetic. Acrylate functions in thick and thin samples show peaks towards 6160 cm^{-1} and 1630 cm^{-1} , respectively, and the epoxide functions show peaks around 3600 cm^{-1} and 790 cm^{-1} for the thick and thin samples, respectively.

2.5. Redox Potentials: Electrochemical Properties

Redox potentials of copper derivatives were determined in DCM by cyclic voltammetry using tetrabutylammonium hexafluorophosphate as the supporting electrolyte (po-

tentials vs. saturated calomel electrode (SCE)). Free energy change (ΔG_{et}) for an electron transfer reaction was calculated from Equation (1) [109], where E_{ox} , E_{red} , E^* and C represent the oxidation potential of the electron donor, the reduction potential of the electron acceptor, the excited-state energy level (determined from fluorescence experiments) and the coulombic term for the initially formed ion pair, respectively. Here, C is neglected as is usually the case for polar solvents.

$$\Delta G_{\text{et}} = E_{\text{ox}} - E_{\text{red}} - E^* + C \quad (1)$$

2.6. UV-Visible Absorption, Steady-State Photolysis and Luminescence Experiments

Acquisition conditions have been detailed elsewhere [13,92,100].

2.7. Computational Procedure

Computational conditions have been detailed elsewhere [13,92,100,110,111]. Simulated absorption spectra of copper complexes were obtained by time-dependent density functional theory at the MPW1PW91/6-31G* level of theory on the relaxed geometries calculated at the UB3LYP/6-31G* level of theory.

2.8. Photocomposite Access Using a Near-UV Conveyor

Photocomposite materials were obtained using a Dymax-UV conveyor at 395 nm. Firstly, photosensitive resins were deposited on the glass fibers (reinforcement), then, this mixture was cured using an LED conveyor @395 nm ($I = 4 \text{ W}\cdot\text{cm}^{-2}$). Distance between the belt and the LED was fixed to 15 mm, and the belt speed was fixed at 2 m/min.

2.9. Direct Laser Write (DLW) Experiment

The photosensitive formulation was deposited on a glass slide and 3D patterns were obtained under air using a computer-controlled diode laser at 405 nm (spot size = 50 μm). Analysis of the 3D patterns was carried out using a numerical optical microscope (DSX-HRSU from OLYMPUS Corporation, Rungis, France) [112].

3. Results

Light-absorption properties, initiation ability and applications (photocomposite synthesis and direct laser write) of the investigated copper complexes will be studied in this section.

3.1. Synthetic Routes to Copper Complexes Cu1 and Cu2

Copper complexes bearing a pyridine-based chelate ligand showed excellent photochemical properties for photocatalysis processes, such as a high-oxidation potential in the excited state [96–99], a long-excited-state lifetime, high-emission quantum yields and high-absorption properties in the UV-visible region. In this work, two new copper complexes have been developed, allowing, by the convenient choice of the ligands, a shift in the absorption properties in the visible range, while maintaining high efficiency.

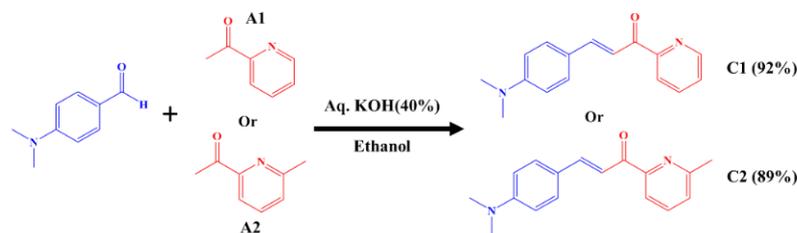
To allow such a shift of the absorption properties towards the visible, two bipyridine ligands were synthesized starting from a chalcone. Structures of these chalcones and, therefore, of the corresponding ligands have been selected in order to induce a significant shift in the absorption spectrum of the copper complexes towards the visible range.

For the synthesis of the two chalcones, a Claisen-Schmidt condensation reaction under basic conditions between 2-acetylpyridine A1 or 2-acetyl-6-methylpyridine A2 and aldehyde A3 was carried out (See Scheme 1) [113–125].

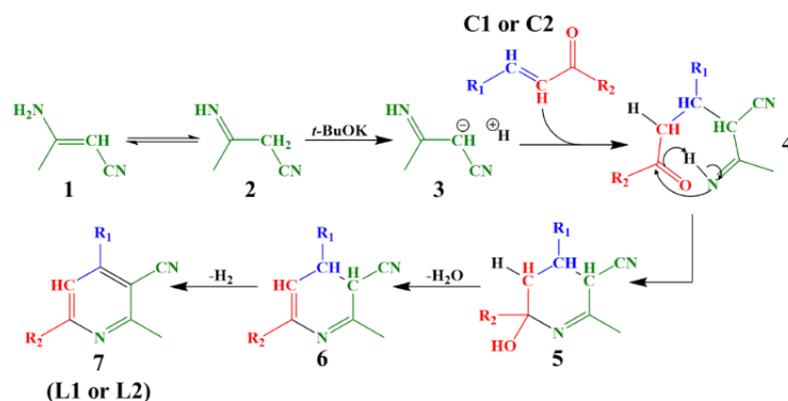
These two chalcones engage in a cyclization reaction with β -aminocrotonitrile, allowing the ligands to be formed. This reaction and its corresponding mechanism were described in the literature in 1992 by Masaki Matsui [105,106].

As shown in Scheme 2, the mechanism proposed by Masaki Matsui involves the formation of two (L1 or L2) ligands. β -Aminocrotonitrile can exist as amino (1) and imino (2)

isomers in solution. A Michael addition of the carbanion of imino isomer 3 to C1 or C2 can give intermediate 4, which, after an intramolecular cyclization and dehydration reaction, can provide intermediate 6. At room temperature, dehydrogenation of 6 can give 7.



Scheme 1. Synthesis and chemical structures of 2-carbonylpyridine-based chalcones.



Scheme 2. Probable mechanism described by Masaki Matsui.

Starting from the conditions described by Masaki Matsui, the ligands were indeed obtained. The synthesis conditions were then optimized by using reduced quantities of solvent, base and β -aminocrotonitrile, and with a simplified reaction treatment due to the precipitation of the ligand at the end of the reaction, while maintaining a good yield. The optimized synthesis of the ligands is detailed in the synthetic procedure detailed above.

Heteroleptic copper complexes bearing a pyridine-based chelate ligand and a diphosphine ligand, such as 4,5-*bis*-(diphenylphosphino)-9,9-dimethylxanthene (or Xantphos) and *bis*[2-(diphenylphosphino)phenyl]ether (or DPEphos), have previously been reported in the literature. In this work, this second ligand was replaced by a bisisonitrile ligand, namely *bis*(2-isocyanophenyl)phenylphosphonate. Indeed, as previously mentioned in a study reported by Matthias Knorn [107], copper complexes bearing this ligand showed a higher photocatalytic activity than their counterpart comprising a bisphosphine ligand. The lower activity of copper complexes comprising bisphosphine ligands can be assigned to the tendency of heteroleptic complexes to form an equilibrium with their homoleptic forms in solution [108], especially for heteroleptic copper complexes combining biphosphine and phenanthroline ligands. In contrast, in the case of the bisisonitrile ligand, studies have revealed the low ability of heteroleptic complexes to undergo ligand exchanges. The ligand was synthesized following the procedure described in the literature. Using these two ligands, the pyridine ligands and the bisisonitrile ligand in a one-step complexation reaction, the two desired copper complexes were obtained.

3.2. UV-Visible Absorption Spectra of Cu1 and Cu2

Ground-state absorption spectra of the new studied copper derivatives were determined in DCM and the results are presented in Figure 3. Extinction coefficients at different emission wavelengths used in photopolymerization experiments are reported in Table 1. New complexes are characterized by a broad absorption band, which extends between 380 nm and 650 nm, and high-extinction coefficients in the blue region,

e.g., $\epsilon = 7570 \text{ M}^{-1}\cdot\text{cm}^{-1}$, $7040 \text{ M}^{-1}\cdot\text{cm}^{-1}$ @400 nm for Cu1 and Cu2, respectively. These compounds also have high-extinction coefficients at the emission wavelengths of LEDs (at 405 nm and 455 nm) used in different experiments achieved in this work, for example, $\epsilon_{@405\text{nm}} = 8460$ and $7950 \text{ M}^{-1}\cdot\text{cm}^{-1}$ for Cu1 and Cu2, respectively. Remarkably, a bathochromic shift in the absorption spectra of Cu2 was observed compared to that of Cu1. This effect could be related to the presence of a methyl group, which is considered as an electron-donating group (inductive effect), on the pyridine ligands of Cu2 ($\lambda_{\text{max}} = 445 \text{ nm}$ for Cu1 and 441 nm for Cu2). This difference could also be explained by the optimized geometries, as well as the frontier orbitals (highest occupied molecular orbital—HOMO—and lowest unoccupied molecular orbital—LUMO), which are shown in Figure 4.

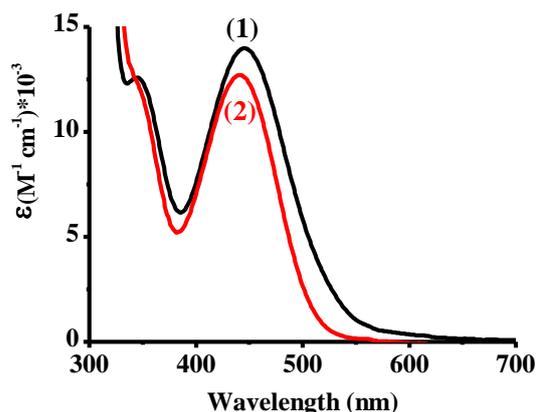


Figure 3. UV-visible absorption spectra of (1) Cu1 and (2) Cu2 in DCM.

Table 1. Maximum absorption wavelengths (λ_{max}), extinction coefficients at λ_{max} , and molar extinction coefficients for the investigated copper complexes at different emission wavelengths for different LEDs used.

	λ_{max} (nm)	ϵ_{max} ($\text{M}^{-1}\cdot\text{cm}^{-1}$)	$\epsilon_{375\text{nm}}$ ($\text{M}^{-1}\cdot\text{cm}^{-1}$)	$\epsilon_{405\text{nm}}$ ($\text{M}^{-1}\cdot\text{cm}^{-1}$)	$\epsilon_{455\text{nm}}$ ($\text{M}^{-1}\cdot\text{cm}^{-1}$)
Cu1	445	14,000	7150	8460	13,600
Cu2	441	12,700	5760	7950	11,740

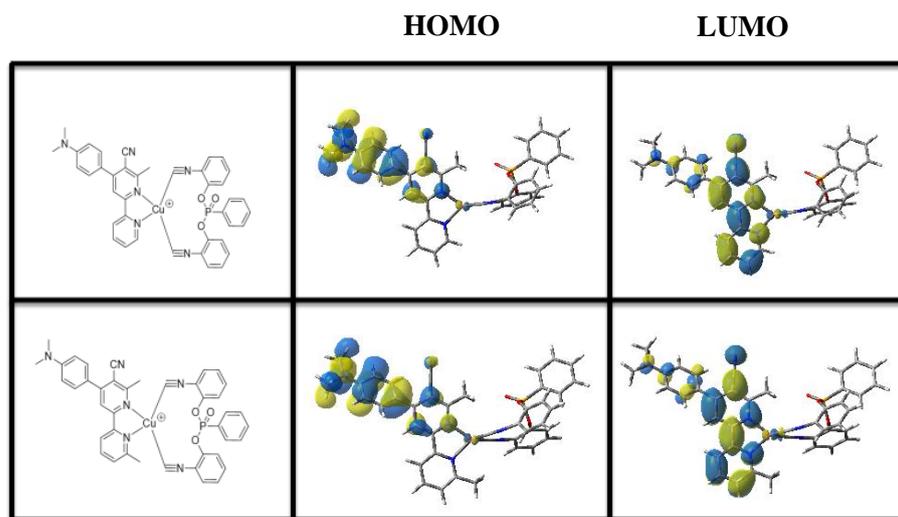


Figure 4. HOMO and LUMO for Cu1 and Cu2 at the UB3LYP/6–31G* level.

3.3. Photopolymerization Experiments

3.3.1. Free Radical Photopolymerization Using TA as a Benchmark Monomer

Due to their good light-absorption properties in the visible range, copper complexes were tested as photoinitiators for the FRP of acrylate-based monomers upon exposure to LEDs at 405 nm ($I = 110 \text{ mW}\cdot\text{cm}^{-2}$) and 455 nm ($I = 75 \text{ mW}\cdot\text{cm}^{-2}$).

In fact, photoinitiators (0.1% or 0.2%) were dissolved and mixed into the TA acrylate monomer in combination with Iod salt (1%) in order to make two-component photoinitiating systems, on the one hand, and in combination with Iod/amine (1%/1% *w/w*) to form three-component photoinitiating systems, on the other hand. Interestingly, these dyes exhibit excellent free radical photopolymerization conversions in thick and thin samples. The related results are gathered in Figure 5 and the data are summarized in Table 2. Remarkably, copper complexes alone, Iod and amine alone cannot polymerize the sample. Iod salt and amine are used as co-initiators in this work because they do not absorb visible light. It is important to introduce the dyes (i.e., the copper complexes) into the photosensitive formulations in order to obtain a good light absorption at 405 nm and 455 nm. The obtained results using copper derivatives in two-component PISs showed that Cu2 was more efficient than Cu1 for the FRP of TA using different PI percentages, e.g., FC ~ 64% for Cu1/Iod (0.1%/1% *w/w*) vs. 70% for Cu2/Iod (0.1%/1% *w/w*) (Figure 5A curve 1 vs. 2), and FC ~ 62% for Cu1/Iod (0.2%/1% *w/w*) vs. 85% for Cu2/Iod (0.2%/1% *w/w*) (Figure 5A curve 3 vs. 4).

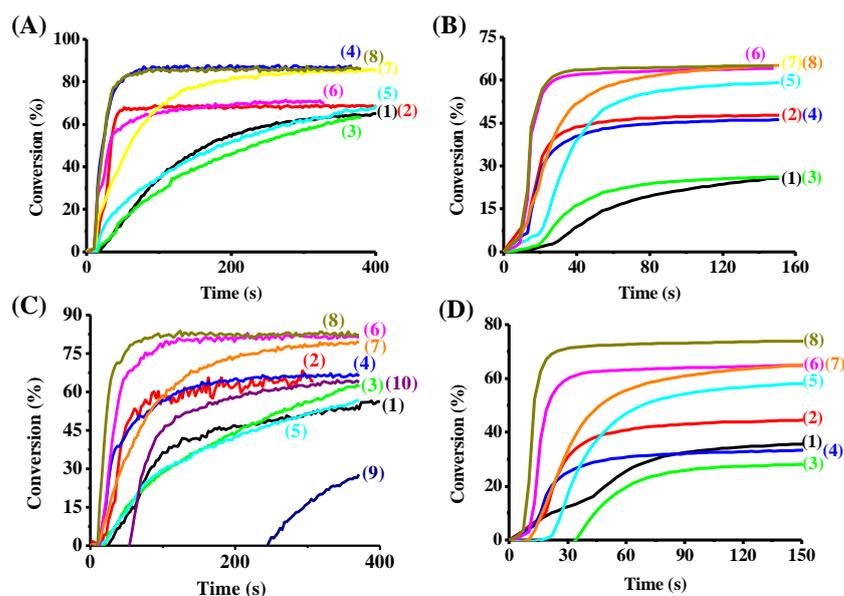


Figure 5. Free radical photopolymerization profiles of acrylate functions vs. irradiation time in: (A) thick samples @455 nm, (B) thin sample @455 nm, (C) thick sample @405 nm and (D) thin sample @405 nm: (1) Cu1/Iod (0.1%/1% *w/w*), (2) Cu2/Iod (0.1%/1% *w/w*), (3) Cu1/Iod (0.2%/1% *w/w*), (4) Cu2/Iod (0.2%/1% *w/w*), (5) Cu1/Iod/EDB (0.1%/1%/1% *w/w/w*), (6) Cu2/Iod/EDB (0.1%/1%/1% *w/w/w*), (7) Cu1/Iod/NPG (0.1%/1%/1% *w/w/w*), (8) Cu2/Iod/NPG (0.1%/1%/1% *w/w/w*), (9) Iod/EDB (1%/1% *w/w*) and (10) Iod/NPG (1%/1% *w/w*). Irradiation starts at $t = 10 \text{ s}$.

Furthermore, Iod/NPG couple showed a weak polymerization initiation ability upon exposure to LEDs at 405 nm and 455 nm after 60 s (e.g., FC ~ 10% @405 nm). Interestingly, a greater efficiency was observed when NPG was incorporated into the formulation. Compared to their two-component system analogues, the different three-component PISs showed a better final conversion of reactive functions and a higher polymerization rate upon irradiation with LEDs at 405 nm or 455 nm (for example, an FC up to 86% is obtained with Cu1/Iod/NPG (0.1%/1%/1% *w/w/w*), and 88% using Cu2/Iod/NPG (0.1%/1%/1% *w/w/w*) with a LED @455 nm).

Table 2. Final reactive functions conversion (FC) for TA monomer using two or three-component PISs upon exposure at different wavelengths (LED at 405 and 455 nm).

	At 405 nm				At 455 nm			
	Thick Sample		Thin Sample		Thick Sample		Thin Sample	
Cu1/Iod	56% ^a	62% ^b	36% ^a	28% ^b	64% ^a	64% ^b	26% ^a	26% ^b
Cu2/Iod	64% ^a	67% ^b	45% ^a	33% ^b	70% ^a	87% ^b	48% ^a	46% ^b
Cu1/Iod/amine	57% ^c	80% ^d	58% ^c	65% ^d	69% ^c	85% ^d	59% ^c	65% ^d
Cu2/Iod/amine	82% ^c	83% ^d	65% ^c	74% ^d	71% ^c	87% ^d	64% ^c	65% ^d

^a: Cu/Iod (0.1%/1% w/w), ^b: Cu/Iod (0.2%/1% w/w), ^c: Cu/Iod/EDB (0.1%/1%/1% w/w/w), ^d: Cu/Iod/NPG (0.1%/1%/1% w/w/w).

3.3.2. Cationic Polymerization and IPN Synthesis

Typical epoxide function conversion-time profiles for Cu1 and Cu2-based photoinitiating systems are given in Figure 6 and the data are gathered in Table 3. In fact, the cationic polymerization of the epoxide functions was carried out under air and upon irradiation at 405 nm. Indeed, the cationic polymerization is insensitive to oxygen. As expected, copper complexes alone and the additives alone were not able to initiate the CP in these irradiation conditions. The addition of Iod salt or Iod/NVK into the formulation containing the PI induced good photopolymerization profiles, i.e., the combination Cu/Iod/NVK (0.1%/2%/3% w/w/w) is very efficient to produce polymer materials in terms of R_p and final epoxy function conversion compared to Cu/Iod (0.1%/1% w/w), e.g., (FC ~ 50% for Cu1/Iod/NVK (0.1%/2%/3% w/w/w) vs. 27% for Cu1/Iod (0.1%/1% w/w)). The consumption of epoxide functions was accompanied by the formation of a polyether network (appearance of peak at $\sim 1080\text{ cm}^{-1}$), characterizing the obtained polymer.

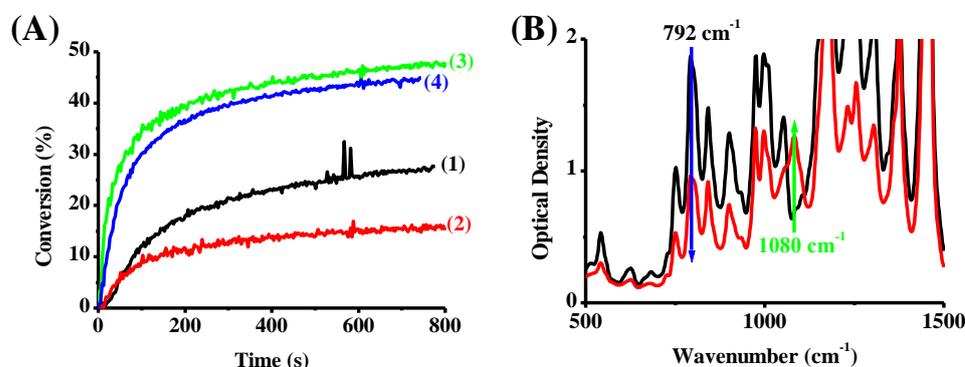


Figure 6. (A) Cationic polymerization (CP) profiles of epoxy functions (thin sample) vs. irradiation time upon exposure to LED at 405 nm: (1) Cu1/Iod (0.1%/1% w/w), (2) Cu2/Iod (0.1%/1% w/w), (3) Cu1/Iod/NVK (0.1%/2%/3% w/w/w) and (4) Cu2/Iod/NVK (0.1%/2%/3% w/w/w). (B) IR spectra recorded before and after polymerization. Irradiation starts at $t = 10$ s.

Table 3. Final reactive function conversions for EPOX monomer using two and three-component PISs upon irradiation at 405 nm during the polymerization of thin samples.

	Cu/Iod (0.1%/1% w/w)	Cu/Iod/NVK (0.1%/2%/3% w/w/w)
Cu1	27%	49%
Cu2	16%	45%

On the other hand, IPNs syntheses were also carried out in this work and polymerization tests were performed in thick and thin samples using LEDs at 405 nm and 455 nm (See Tables 4 and 5). Photopolymerization profiles for the IPN formation are presented in Figure 7. For example, the acrylic network formation was very fast with a high final conversion (98%) for Cu2/Iod/NPG (0.1%/1%/1% w/w/w) in TA/EPOX (50%/50%) upon

irradiation at 455 nm, and the formation of the epoxy network was also efficient (high final conversion and R_p) using this system (FC ~ 55%).

Table 4. Final conversions of acrylate and epoxides functions for the IPN synthesis of TA/EPOX blend using Cu1 (or Cu2)/Iod/NPG (0.1%/1%/1% w/w/w) as PIS upon exposure to visible light at 405 nm.

	IPN Synthesis of TA/EPOX Blend Performed in Thick Sample at 405 nm			IPN Synthesis of TA/EPOX Blend Performed in Thin Sample at 405 nm		
	30%/70%	50%/50%	70%/30%	30%/70%	50%/50%	70%/30%
Cu1	90%/25%	90%/15%	93%/27%	88%/25%	87%/31%	84%/47%
Cu2	99%/30%	98%/20%	96%/38%	92%/22%	90%/35%	80%/32%

Table 5. Final conversions of acrylate and epoxides functions for the IPN synthesis of TA/EPOX blend using Cu1 (or Cu2)/Iod/NPG (0.1%/1%/1% w/w/w) as PIS upon exposure to visible light at 455 nm.

	IPN Synthesis of TA/EPOX Blend Performed in Thick Sample @455 nm			IPN Synthesis of TA/EPOX Blend Performed in Thin Sample @455 nm		
	30%/70%	50%/50%	70%/30%	30%/70%	50%/50%	70%/30%
Cu1	90%/30%	90%/23%	90%/41%	90%/15%	90%/25%	90%/15%
Cu2	100%/38%	98%/55%	99%/51%	98%/22%	99%/30%	98%/22%

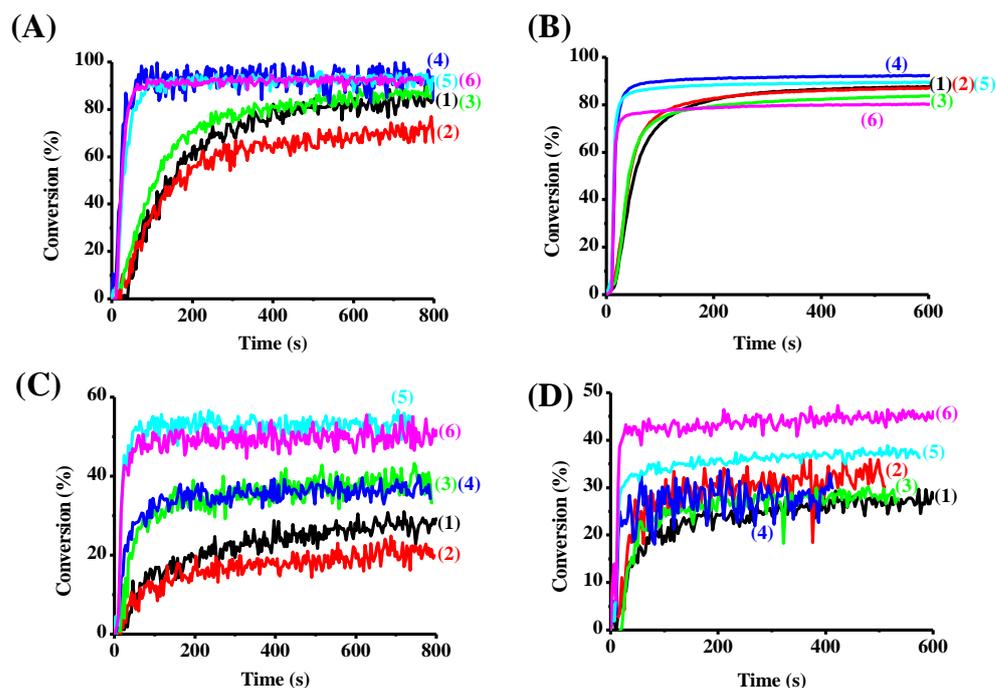


Figure 7. Photopolymerization profiles of acrylate functions (A) (thick sample), (B) (thin sample)) upon irradiation at 455 nm, and epoxide function ((C) (thick sample), (D) (thin sample)) upon exposure to LED at 405 nm of TA/EPOX using Cu1/Iod/NPG (0.1%/1%/1% w/w/w): (1) 30%/70%, (2) 50%/50%, (3) 70%/30%, and Cu2/Iod/NPG (0.1%/1%/1% w/w/w): (4) 30%/70%, (5) 50%/50%, (6) 70%/30%. The irradiation starts at $t = 10$ s.

3.4. Photocomposites Synthesis

Nowadays, many of our modern technologies require materials with enhanced properties. This is particularly true for materials used in aerospace, underwater and transportation applications. For example, for aeronautical applications, engineers research materials with properties of low density, rigid, solid, impact resistance, temperature and pressure resistance and obviously materials that do not easily corrode. For this purpose, composite

materials have been used for different applications. By definition, a composite material is composed of a least two components that results in better properties than those of the individual components used alone: matrix (monomer blends) and reinforcement. The main advantages of composite materials are their high stiffness, strength and low density. The introduction of light for the synthesis of photocomposites will make the manufacture of these materials more ecological.

In this study, the matrix is based on acrylic monomers, such as TMPTA or TA, and the second component (reinforcement) is based on glass fibers. Firstly, the acrylic resins were deposited on the reinforcement (50%/50% *w/w*) and the mixtures were irradiated using an LED conveyor at 395 nm. Interestingly, a very fast polymerization on the surface and the bottom was observed with tack-free surfaces, after one pass only using one layer of glass fibers (1 mm). Increasing the reinforcement thickness by adding several layers, the polymerization on the surface is always fast and takes place after one pass, but the curing on the bottom is more complicated and will be done after several passes using Cu1 or Cu2/Iod/NPG (0.1%/1%/1% *w/w/w*) as PISs. The curing photocomposite results are depicted in Figure 8 and Table 6.

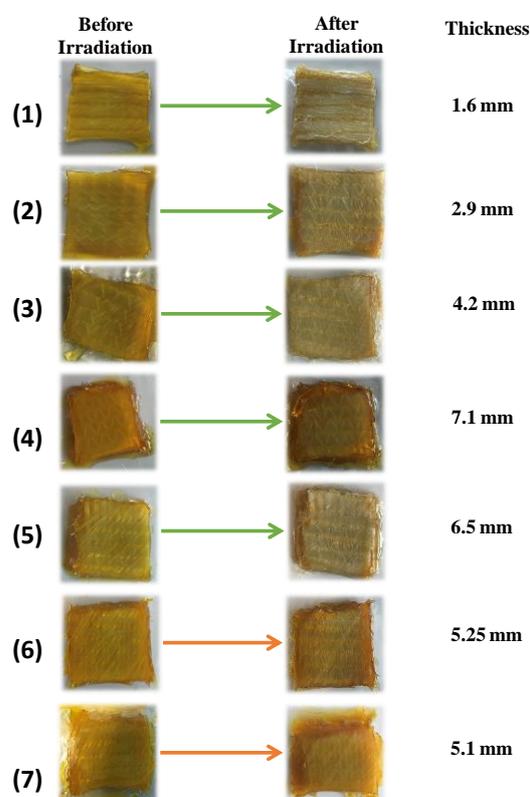


Figure 8. Free radical photopolymerization for the photocomposite synthesis upon near-UV irradiation at 395 nm ($4 \text{ W} \cdot \text{cm}^{-2}$) using Cu2/Iod/NPG (0.1%/1%/1% *w/w/w*) in TA [(1)–(4)], (5) Cu2/Iod/NPG (0.1%/1%/1% *w/w/w*) in TMPTA, (6) Cu1/Iod/NPG (0.1%/1%/1% *w/w/w*) in TMPTA and (7) Cu1/Iod/NPG (0.1%/1%/1% *w/w/w*) in TA.

3.5. Direct Laser Write (DLW)

The new copper complexes were tested in some direct laser write experiments for the FRP of TMPTA or TA using a laser diode at 405 nm (spot size: 50 μm). The obtained 3D patterns were carried out under air and using different PISs based on Cu1/Iod/TMA, Cu2/Iod/TMA in TA or TMPTA (Figure 9). Due to their high ability to initiate the FRP of acrylates, these systems were able to generate high-spatial-resolution 3D patterns with a great thickness of curing ($\sim 2500 \mu\text{m}$) in the irradiated area. As such, 3D patterns were

generated with very short irradiation times (2–3 min) and they were characterized by numerical microscopy.

Table 6. Photocomposite synthesis results using TA as acrylic monomer (or TMPTA) and number of passes to reach the tack-free character on the surfaces.

	Thickness	Number of Passes to Reach Tack-Free Character on the Surface	Number of Passes to Reach Tack-Free Character on the Bottom
Cu2/Iod/NPG	1.6 mm	1	1
Cu2/Iod/NPG	2.9 mm	1	2
Cu2/Iod/NPG	4.2 mm	1	6
Cu2/Iod/NPG (TMPTA)	7.1 mm	1	25
Cu2/Iod/NPG	6.5 mm	1	30
Cu1/Iod/NPG	5.25 mm	1	40
Cu1/Iod/NPG (TMPTA)	5.1 mm	1	45

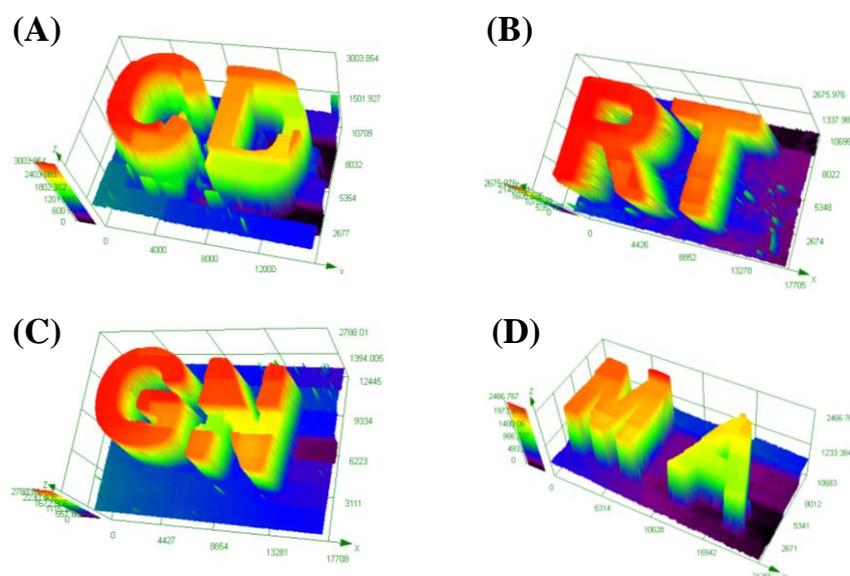


Figure 9. 3D patterns produced by free radical photopolymerization of acrylate functions (TA or TMPTA) using a laser diode at 405 nm and their characterization by numerical optical microscopy: (A) Cu2/Iod/TMA (0.057%/1%/0.46% *w/w/w*) in TA, (B) Cu1/Iod/TMA (0.058%/0.506%/0.44% *w/w/w*) in TMPTA; (C) Cu2/Iod/TMA (0.048%/0.65%/0.259% *w/w/w*) in TA and (D) Cu1/Iod/TMA (0.05%/0.5%/0.305% *w/w/w*).

3.6. Mechanical Properties: Tensile Test Measurements

The tensile strength of IPNs synthesized using different compositions of the TA/EPOX mixture are presented in Table 7. The results show that with the increase in the percentage of acrylic monomer, the tensile strength increases, which may be due to the rigid character of the acrylates (e.g., 7.2 MPa for Cu2/Iod/NPG in TA/EPOX (30%/70%) vs. 37.2 MPa for the same system in TA/EPOX (70%/30%).

Table 7. The tensile strength of IPN materials as a result of hybrid polymerization of the TA/EPOX mixture using Cu/Iod/NPG (0.1%/1%/1% *w/w/w*) as a photoinitiating system.

Tensile Strength [MPa]	0.1% PA/Iod/NPG TA/EPOX (30% 70%) @ 395 nm	0.1% PA/Iod/NPG TA/EPOX (50% 50%) @ 395 nm	0.1% PA/Iod/NPG TA/EPOX (70% 30%) @ 395 nm
Cu1	6.5	7.3	34.3
Cu 2	7.2	26.3	37.2

4. Discussion

In order to explain the initiating ability of the organometallic complexes, their photochemical and photophysical properties were studied using different characterization techniques, allowing for the characterization of the associated chemical mechanisms.

4.1. Steady-State Photolysis of the Investigated Compounds

Photolyses of Cu1 and Cu2 dyes in DCM were investigated upon irradiation at 375 nm and 405 nm, and the related results are shown in Figure 10. First of all, no photolysis occurred for Cu1 and Cu2 alone (0% consumption) upon irradiation at 375 nm and 405 nm, but the incorporation of the iodonium salt into the photosensitive solution could promote the degradation of the dyes, so that a strong decrease in the absorbance band intensity was observed by increasing the irradiation time, e.g., consumption $\sim 80\%$ @375 nm and 82% for Cu2/Iod at 375 nm and 405 nm, respectively (Figure 11B). It is important to note that the photolysis of Cu1 in the presence of Iod salt involved the formation of a photoproduct after 60 s of irradiation in the solution, which had an absorption band more shifted in the visible (bathochromic effect) spectrum, then this photoproduct degrades under the effect of the irradiation (Figure 10A).

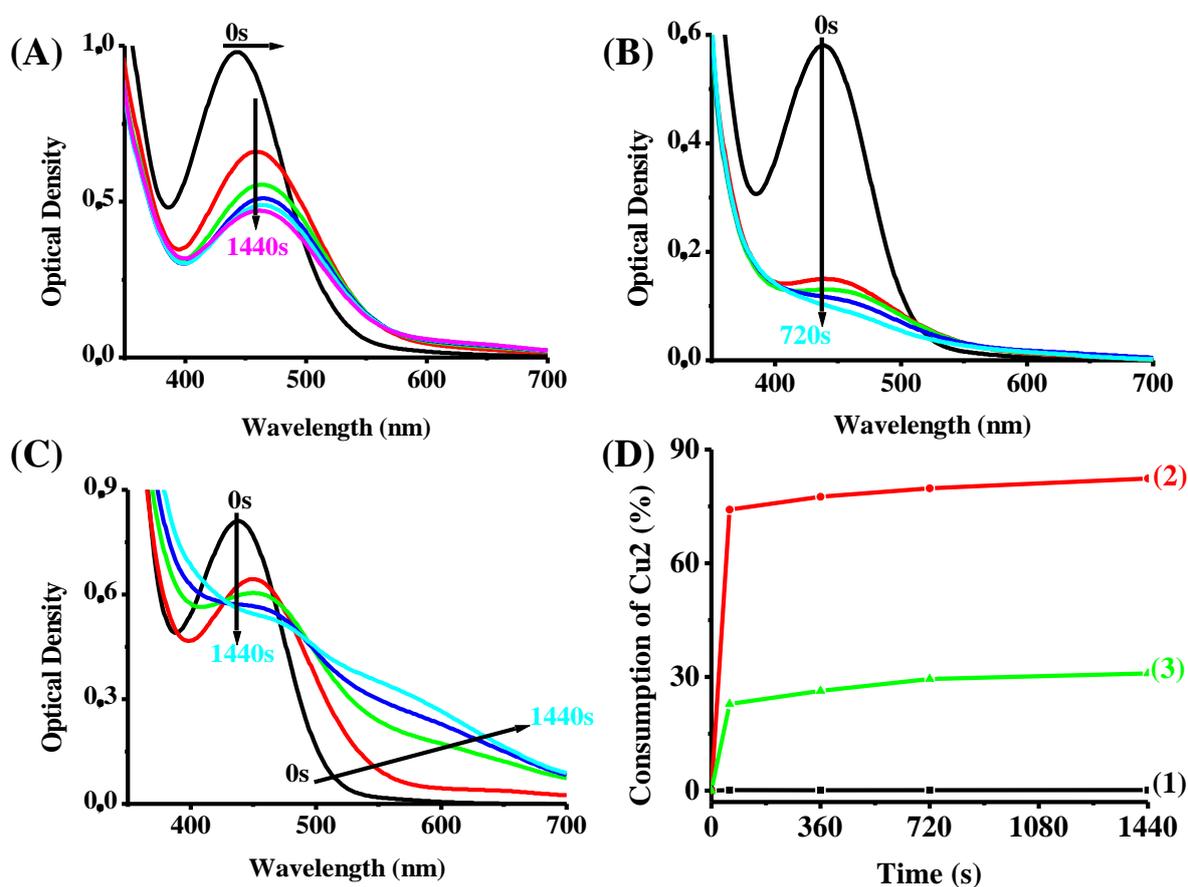


Figure 10. Photolysis experiments of (A) Cu1 with Iod salt (10^{-2} M), (B) Cu2 with Iod salt (10^{-2} M) and (C) Cu2/Iod/NPG (10^{-2} M) upon exposure to LED at 405 nm. (D) Consumption percentage of Cu2: (1) alone, (2) with Iod, (3) with Iod/NPG.

This difference between these two consumption percentages may be due to the high light-absorption ability of Cu2 at 405 nm, as well as the highest intensity of the LED at 405 nm ($110 \text{ mW}\cdot\text{cm}^{-2}$), compared to that at 375 nm ($75 \text{ mW}\cdot\text{cm}^{-2}$). Furthermore, in the case of three-component PISs, the consumption of Cu2 was lower compared to that of the two-component Cu2/Iod system. It can be confidently assigned to the regeneration of Cu2

in the three-component system due to the presence of the sacrificial amine or the formation of new photoproducts (%consumption ~ 31%).

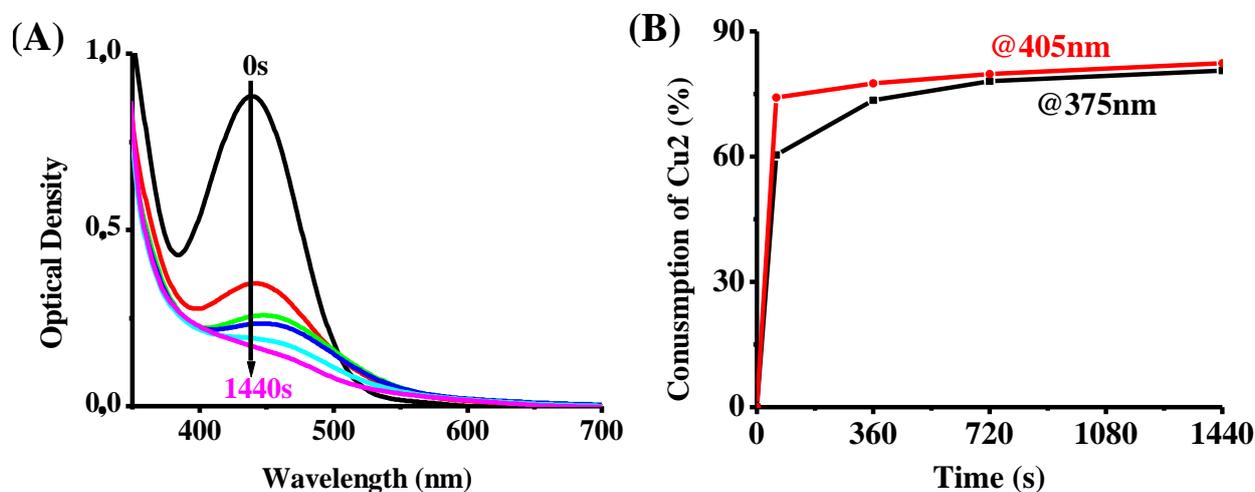


Figure 11. (A) Photolysis of Cu₂ with Iod (10^{-2} M) upon irradiation @375 nm. (B) Consumption of Cu₂ with irradiation @375 nm and 405 nm.

4.2. Photoluminescence and Electrochemical Properties

Fluorescence emission spectra, fluorescence quenching (measured using a JASCO FP-6200 spectrofluorimeter, Lisses, France) and the oxidation potential (measured in DCM by cyclic voltammetry, OrigaLys, Rillieux-la-Pape, France) results of the different Cu derivatives are gathered in Figure 12 and Table 8. The excited-state energy was calculated from the crossing point of the emission and absorption spectra. Using these different values, the free-energy change (ΔG) could be calculated; this parameter reflects the reactivity between Cu and Iod. In fact, a slight decrease in the fluorescence intensity was observed for Cu₁/Iod, but this emission spectra showed a strong decrease for Cu₂ upon addition of Iod. These behaviors explain the high reactivity of Cu₂/Iod compared to Cu₁/Iod e.g., $\phi = 0.55$ for Cu₁/Iod vs. 0.74 for Cu₂/Iod. In addition, the ΔG value is negative for both complexes, so that the photo-oxidation interaction Cu₁ (or Cu₂)/Iod is favorable in both cases, with a superiority observed for Cu₂ ($\Delta G = -0.74$ and 0.62 eV for Cu₂ and Cu₁, respectively). It, therefore, explains the high-photoinitiation ability of Cu₂ compared to Cu₁.

Finally, the initiation ability of the new copper complexes could be explained by different characterization techniques, which allowed us to propose a chemical photoinitiation mechanism. Firstly, Cu is excited upon irradiation at 405 or 455 nm and interacts with Iod to generate aryl radical (Ar^{\bullet}) and radical $Cu^{\bullet+}$ [r1–r2]. A charge transfer complex CTC can be formed after adding NPG into the photosensitive formulation. This complex is able to produce aryl radicals as active species for the radical photopolymerization [r3–r4]. Then, $^{1,3}Cu$ could react with NPG and generate two radicals (NPG_{-H}^{\bullet} , $Cu-H^{\bullet}$) [r5], and the first radical can undergo a decarboxylation and produce active radicals ($NPG_{(-H,-CO_2)}^{\bullet}$) [r6]. This radical can also lead to the formation of two active species after interaction with Iod salt ($NPG_{(-H,-CO_2)}^+$, Ar^{\bullet}) [r7]. Lastly, copper complex derivatives are regenerated [r8–r9] (See Scheme 3).

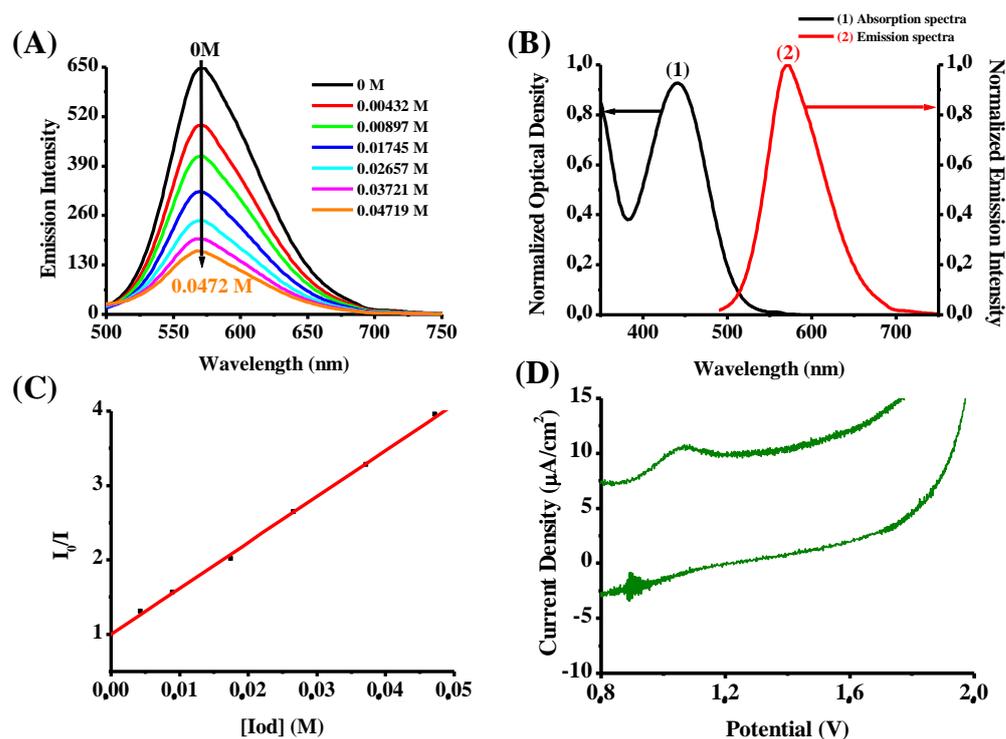
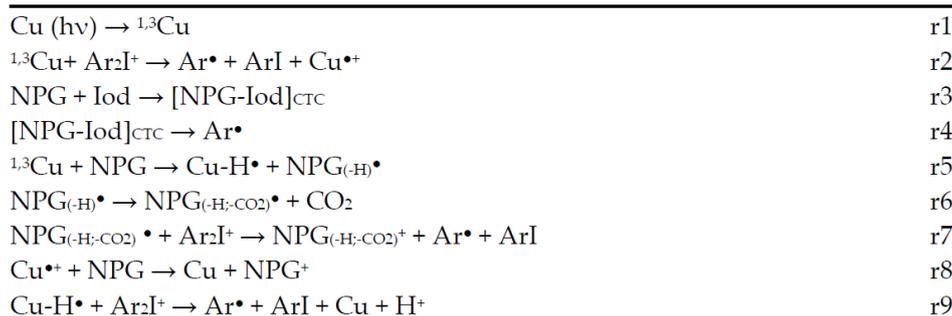


Figure 12. (A) Fluorescence quenching of Cu₂ by Iod salt, (B) E_{S1} determination for Cu₂, (C) Stern–Volmer coefficient determination of Cu₂ quenched by Iod and (D) oxidation potential determination of Cu₂.

Table 8. Parameters characterizing the chemical mechanisms between Cu₁ (or Cu₂) and Iod. For Iod, a reduction potential of -0.7 eV was used for the ΔG_{et} calculations.

	E _{ox} (V)	E _{S1} (eV)	$\Delta G_{(Cu/Iod)}$ (eV)	K _{SV(Cu/Iod)}	$\Phi_{(Cu/Iod)}$	E _{ox} (V)
Cu ₁	1.07	2.34	-0.62	13.58	0.55	Cu ₁
Cu ₂	0.97	2.41	-0.74	61.83	0.74	Cu ₂



Scheme 3. Proposed chemical mechanisms.

5. Conclusions

In the present paper, new copper complexes were synthesized and tested as photoinitiators. These compounds have strong visible-light absorption and are able to initiate both the free radical photopolymerization and cationic polymerization. IPN synthesis through the simultaneous polymerization of acrylate/epoxy monomer blends was performed under air upon irradiation at 405 nm and 455 nm, using a very low quantity of copper complex, in two or three-component PIS. Cu₂ showed a very interesting photoinitiation capacity compared to Cu₁ in terms of final conversions of reactive functions and polymerization

rates. The high reactivity of these compounds was demonstrated through some direct laser write experiments, where high-spatial-resolution 3D patterns were obtained. In addition, the synthesis of thick glass fiber photocomposites was possible. This work paves the way for the development of new organometallic photoinitiators.

Author Contributions: Conceptualization, F.D. and J.L.; methodology, M.R., G.N., B.G., J.T., T.H., D.G., F.D. and J.L.; software, B.G.; validation, M.R., G.N., B.G., J.T., T.H., D.G., F.D. and J.L.; formal analysis, M.R., G.N., B.G., J.T., T.H., D.G., F.D. and J.L.; investigation, M.R., G.N., B.G., J.T., T.H., D.G., F.D. and J.L.; resources, F.D. and J.L.; data curation, F.D. and J.L.; writing—original draft preparation, M.R., G.N., B.G., J.T., T.H., D.G., F.D. and J.L.; writing—review and editing, M.R., G.N., B.G., J.T., T.H., D.G., F.D. and J.L.; visualization, F.D.; supervision, M.R., G.N., B.G., J.T., T.H., D.G., F.D. and J.L.; project administration, M.R., G.N., B.G., J.T., T.H., D.G., F.D. and J.L.; funding acquisition, M.R., G.N., B.G., J.T., T.H., D.G., F.D. and J.L. All authors have read and agreed to the published version of the manuscript.

Funding: This research was funded by Aix Marseille University and the Centre National de la Recherche Scientifique.

Data Availability Statement: Not applicable.

Conflicts of Interest: The authors declare no conflict of interest.

References

1. Fouassier, J.P.; Lalevée, J. *Photoinitiators for Polymer Synthesis, Scope, Reactivity, and Efficiency*; Wiley-VCH Verlag: Weinheim, Germany, 2012.
2. Fouassier, J.P. *Photoinitiator, Photopolymerization and Photocuring: Fundamentals and Applications*; Hanser Publishers: Munich, Germany, 1995.
3. Dietliker, K.A. *Compilation of Photoinitiators Commercially Available for UV Today*; Sita Technology Ltd.: London, UK, 2002.
4. Davidson, S. *Exploring the Science, Technology and Application of UV and EB Curing*; Sita Technology Ltd.: London, UK, 1999.
5. Crivello, J.V.; Dietliker, K.; Bradley, G. *Photoinitiators for Free Radical Cationic & Anionic Photopolymerisation*; John Wiley & Sons: Chichester, UK, 1999.
6. Cunningham, A.F.; Desobry, V. *Radiation Curing in Polymer Science and Technology*; Fouassier, J.P., Rabek, J.F., Eds.; Elsevier: Barking, UK, 1993; Volume 2, p. 323.
7. Andrzejewska, E. Chapter 2—Free Radical Photopolymerization of Multifunctional Monomers. In *Three-Dimensional Microfabrication Using Two-Photon Polymerization*; Baldacchini, T., Ed.; Micro and Nano Technologies; William Andrew Publishing: Oxford, UK, 2016; pp. 62–81. ISBN 978-0-323-35321-2.
8. Luu, T.T.H.; Jia, Z.; Kanaev, A.; Museur, L. Effect of Light Intensity on the Free-Radical Photopolymerization Kinetics of 2-Hydroxyethyl Methacrylate: Experiments and Simulations. *J. Phys. Chem. B* **2020**, *124*, 6857–6866. [[CrossRef](#)] [[PubMed](#)]
9. Andrezajewska, E.; Grajek, K. Recent Advances in Photo-Induced Free-Radical Polymerization. *MOJ Polym. Sci.* **2017**, *1*, 58–60. [[CrossRef](#)]
10. Li, Z.; Zou, X.; Shi, F.; Liu, R.; Yagci, Y. Highly Efficient Dandelion-like near-Infrared Light Photoinitiator for Free Radical and Thiol-Ene Photopolymerizations. *Nat. Commun.* **2019**, *10*, 3560. [[CrossRef](#)] [[PubMed](#)]
11. Sangermano, M.; Roppolo, I.; Chiappone, A. New Horizons in Cationic Photopolymerization. *Polymers* **2018**, *10*, 136. [[CrossRef](#)]
12. Zhou, Y.; Liao, W.; Ni, X. Cationic Photopolymerization Initiated by a Photocatalytic Complex Sensitive to Visible Light at 520 Nm. *Catal. Lett.* **2021**, *151*, 1766–1775. [[CrossRef](#)]
13. Bouzrati-Zerelli, M.; Maier, M.; Dietlin, C.; Morlet-Savary, F.; Fouassier, J.P.; Klee, J.E.; Lalevée, J. A novel photoinitiating system producing germyl radicals for the polymerization of representative methacrylate resins: Camphorquinone/R3GeH/iodonium salt. *Dent. Mater.* **2016**, *32*, 1226. [[CrossRef](#)]
14. Abdul-Monem, M.M. Naturally Derived Photoinitiators for Dental and Biomaterials Applications. *Eur. Dent. Res. Biomater. J.* **2021**, *1*, 72–78. [[CrossRef](#)]
15. Alizadehgharib, S.; Östberg, A.-K.; Dahlstrand Rudin, A.; Dahlgren, U.; Christenson, K. The Effects of the Dental Methacrylates TEGDMA, Bis-GMA, and UDMA on Neutrophils in Vitro. *Clin. Exp. Dent. Res.* **2020**, *6*, 439–447. [[CrossRef](#)]
16. Arikawa, H.; Takahashi, H.; Kanie, T.; Ban, S. Effect of Various Visible Light Photoinitiators on the Polymerization and Color of Light-Activated Resins. *Dent. Mater. J.* **2009**, *28*, 454–460. [[CrossRef](#)]
17. Catarzi, D.; Cecchi, L.; Colotta, V.; Melani, F.; Filacchioni, G.; Martini, C.; Giusti, L.; Lucacchini, A. Structure-Activity Relationships of 1,2,4-Triazolo [1,5-a]Quinoxalines and Their 1-Deaza Analogs Imidazo [1,2-a]Quinoxalines at the Benzodiazepine Receptor. *J. Med. Chem.* **1994**, *37*, 2846–2850. [[CrossRef](#)]
18. Boeira, P.O.; Meereis, C.T.W.; Suárez, C.E.C.; de Almeida, S.M.; Piva, E.; da Silveira Lima, G. Coumarin-Based Iodonium Hexafluoroantimonate as an Alternative Photoinitiator for Experimental Dental Adhesives Resin. *Appl. Adhes. Sci.* **2017**, *5*, 2. [[CrossRef](#)]

19. Cadenaro, M.; Antonioli, F.; Codan, B.; Agee, K.; Tay, F.R.; Dorigo, E.D.S.; Pashley, D.H.; Breschi, L. Influence of Different Initiators on the Degree of Conversion of Experimental Adhesive Blends in Relation to Their Hydrophilicity and Solvent Content. *Dent. Mater.* **2010**, *26*, 288–294. [[CrossRef](#)] [[PubMed](#)]
20. Dickens, S.H.; Stansbury, J.W.; Choi, K.M.; Floyd, C.J.E. Photopolymerization Kinetics of Methacrylate Dental Resins. *Macromolecules* **2003**, *36*, 6043–6053. [[CrossRef](#)]
21. Ikemura, K.; Endo, T. A Review of the Development of Radical Photopolymerization Initiators Used for Designing Light-Curing Dental Adhesives and Resin Composites. *Dent. Mater. J.* **2010**, *29*, 481–501. [[CrossRef](#)]
22. Maffezzoli, A.; Pietra, A.D.; Rengo, S.; Nicolais, L.; Valletta, G. Photopolymerization of Dental Composite Matrices. *Biomaterials* **1994**, *15*, 1221–1228. [[CrossRef](#)]
23. Neumann, M.G.; Schmitt, C.C.; Ferreira, G.C.; Corrêa, I.C. The Initiating Radical Yields and the Efficiency of Polymerization for Various Dental Photoinitiators Excited by Different Light Curing Units. *Dent. Mater.* **2006**, *22*, 576–584. [[CrossRef](#)]
24. Maruno, T.; Murata, N. Properties of a UV-Curable, Durable Precision Adhesive. *J. Adhes. Sci. Technol.* **1995**, *9*, 1343. [[CrossRef](#)]
25. Besse, V.; Derbanne, M.A.; Pham, T.-N.; Cook, W.D.; Le Pluart, L. Photopolymerization Study and Adhesive Properties of Self-Etch Adhesives Containing Bis(Acyl)Phosphine Oxide Initiator. *Dent. Mater.* **2016**, *32*, 561–569. [[CrossRef](#)]
26. Gziut, K.; Kowalczyk, A.; Schmidt, B.; Kowalczyk, K.; Weisbrodt, M. Epoxy-Based Structural Self-Adhesive Tapes Modified with Acrylic Syrups Prepared via a Free Radical Photopolymerization Process. *Polymers* **2021**, *13*, 189. [[CrossRef](#)]
27. Zhu, M.; Cao, Z.; Zhou, H.; Xie, Y.; Li, G.; Wang, N.; Liu, Y.; He, L.; Qu, X. Preparation of Environmentally Friendly Acrylic Pressure-Sensitive Adhesives by Bulk Photopolymerization and Their Performance. *RSC Adv.* **2020**, *10*, 10277–10284. [[CrossRef](#)]
28. Kilponen, L.; Uusitalo, E.; Tolvanen, M.; Varrelä, J.; Vallittu, P.K. Photopolymerization of Light Curing Adhesives Used with Metal Orthodontic Brackets and Matrices. *J. Biomater. Tissue Eng.* **2016**, *6*, 659–664. [[CrossRef](#)]
29. Wu, L.; Baghdachi, J. *Functional Polymer Coatings: Principles, Methods, and Applications*; Wiley Series on Polymer Engineering and Technology: New York, NY, USA, 2015.
30. Al Rashid, A.; Ahmed, W.; Khalid, M.Y.; Koç, M. Vat Photopolymerization of Polymers and Polymer Composites: Processes and Applications. *Addit. Manuf.* **2021**, *47*, 102279. [[CrossRef](#)]
31. Pagac, M.; Hajnys, J.; Ma, Q.-P.; Jancar, L.; Jansa, J.; Stefek, P.; Mesicek, J. A Review of Vat Photopolymerization Technology: Materials, Applications, Challenges, and Future Trends of 3D Printing. *Polymers* **2021**, *13*, 598. [[CrossRef](#)] [[PubMed](#)]
32. Noè, C.; Hakkarainen, M.; Malburet, S.; Graillot, A.; Adekunle, K.; Skrifvars, M.; Sangermano, M. Frontal-Photopolymerization of Fully Biobased Epoxy Composites. *Macromol. Mater. Eng.* **2021**, 2100864. [[CrossRef](#)]
33. Dikova, T.; Maximov, J.; Todorov, V.; Georgiev, G.; Panov, V. Optimization of Photopolymerization Process of Dental Composites. *Processes* **2021**, *9*, 779. [[CrossRef](#)]
34. Mokbel, H.; Anderson, D.; Plenderleith, R.; Dietlin, C.; Morlet-Savary, F.; Dumur, F.; Gignes, D.; Fouassier, J.P.; Lalevée, J. Copper Photoredox Catalyst “G1”: A New High Performance Photoinitiator for near-UV and Visible LEDs. *Polym. Chem.* **2017**, *8*, 5580. [[CrossRef](#)]
35. Pereira, R.F.; Bártolo, P.J. Photopolymerizable hydrogels in regenerative medicine and drug delivery. In *Hot Topics in Biomaterials; Future Science Book Series Volume 6*; Future Science Ltd.: London, UK, 2014.
36. Xu, X.; Awad, A.; Robles-Martinez, P.; Gaisford, S.; Goyanes, A.; Basit, A.W. Vat Photopolymerization 3D Printing for Advanced Drug Delivery and Medical Device Applications. *J. Control. Release* **2021**, *329*, 743–757. [[CrossRef](#)]
37. Chiulan, I.; Heggset, E.B.; Voicu, Ş.I.; Chinga-Carrasco, G. Photopolymerization of Bio-Based Polymers in a Biomedical Engineering Perspective. *Biomacromolecules* **2021**, *22*, 1795–1814. [[CrossRef](#)]
38. Elisseeff, J.; Anseth, K.; Sims, D.; McIntosh, W.; Randolph, M.; Langer, R. Transdermal Photopolymerization for Minimally Invasive Implantation. *Proc. Natl. Acad. Sci. USA* **1999**, *96*, 3104–3107. [[CrossRef](#)]
39. Bao, Y.; Paunović, N.; Leroux, J.-C. Challenges and Opportunities in 3D Printing of Biodegradable Medical Devices by Emerging Photopolymerization Techniques. *Adv. Funct. Mater.* **2022**, *32*, 2109864. [[CrossRef](#)]
40. Baroli, B. Photopolymerization of Biomaterials: Issues and Potentialities in Drug Delivery, Tissue Engineering, and Cell Encapsulation Applications. *J. Chem. Technol. Biotechnol.* **2006**, *81*, 491–499. [[CrossRef](#)]
41. Lee, J.Y.; An, J.; Chua, C.K. Fundamentals and Applications of 3D Printing for Novel Materials. *Appl. Mater. Today.* **2017**, *7*, 120. [[CrossRef](#)]
42. Andreu, A.; Su, P.-C.; Kim, J.-H.; Ng, C.S.; Kim, S.; Kim, I.; Lee, J.; Noh, J.; Subramanian, A.S.; Yoon, Y.-J. 4D Printing Materials for Vat Photopolymerization. *Addit. Manuf.* **2021**, *44*, 102024. [[CrossRef](#)]
43. Bagheri, A.; Jin, J. Photopolymerization in 3D Printing. *ACS Appl. Polym. Mater.* **2019**, *1*, 593–611. [[CrossRef](#)]
44. Tang, Y.; Dai, B.; Su, B.; Shi, Y. Recent Advances of 4D Printing Technologies Toward Soft Tactile Sensors. *Front. Mater.* **2021**, *8*, 658046. [[CrossRef](#)]
45. Imrie, P.; Jin, J. Polymer 4D Printing: Advanced Shape-Change and Beyond. *J. Polym. Sci.* **2022**, *60*, 149–174. [[CrossRef](#)]
46. Zhang, Z.; Corrigan, N.; Bagheri, A.; Jin, J.; Boyer, C. A Versatile 3D and 4D Printing System through Photocontrolled RAFT Polymerization. *Angew. Chem.* **2019**, *131*, 18122–18131. [[CrossRef](#)]
47. Schwartz, J.J.; Boydston, A.J. Multimaterial Actinic Spatial Control 3D and 4D Printing. *Nat. Commun.* **2019**, *10*, 791. [[CrossRef](#)]
48. Jeong, H.Y.; Woo, B.H.; Kim, N.; Jun, Y.C. Multicolor 4D Printing of Shape-Memory Polymers for Light-Induced Selective Heating and Remote Actuation. *Sci. Rep.* **2020**, *10*, 6258. [[CrossRef](#)]

49. Shan, W.; Chen, Y.; Hu, M.; Qin, S.; Liu, P. 4D Printing of Shape Memory Polymer via Liquid Crystal Display (LCD) Stereolithographic 3D Printing. *Mater. Res. Express* **2020**, *7*, 105305. [CrossRef]
50. Choong, Y.Y.C.; Maleksaeedi, S.; Eng, H.; Yu, S.; Wei, J.; Su, P.-C. High Speed 4D Printing of Shape Memory Polymers with Nanosilica. *Appl. Mater. Today* **2020**, *18*, 100515. [CrossRef]
51. Tedla, G.; Jarabek, A.M.; Byrley, P.; Boyes, W.; Rogers, K. Human Exposure to Metals in Consumer-Focused Fused Filament Fabrication (FFF)/ 3D Printing Processes. *Sci. Total Environ.* **2022**, *814*, 152622. [CrossRef]
52. Pierau, L.; Elian, C.; Akimoto, J.; Ito, Y.; Caillol, S.; Versace, D.-L. Bio-Sourced Monomers and Cationic Photopolymerization—The Green Combination towards Eco-Friendly and Non-Toxic Materials. *Prog. Polym. Sci.* **2022**, *127*, 101517. [CrossRef]
53. Leonhardt, S.; Klare, M.; Scheer, M.; Fischer, T.; Cordes, B.; Eblenkamp, M. Biocompatibility of Photopolymers for Additive Manufacturing. *Curr. Dir. Biomed. Eng.* **2016**, *2*, 113–116. [CrossRef]
54. Klikovits, N.; Knaack, P.; Bomze, D.; Krossing, I.; Liska, R. Novel Photoacid Generators for Cationic Photopolymerization. *Polym. Chem.* **2017**, *8*, 4414–4421. [CrossRef]
55. Mueller, M.; Bandl, C.; Kern, W. Surface-Immobilized Photoinitiators for Light Induced Polymerization and Coupling Reactions. *Polymers* **2022**, *14*, 608. [CrossRef]
56. Zhou, J.; Allonas, X.; Ibrahim, A.; Liu, X. Progress in the Development of Polymeric and Multifunctional Photoinitiators. *Prog. Polym. Sci.* **2019**, *99*, 101165. [CrossRef]
57. Tomal, W.; Ortyl, J. Water-Soluble Photoinitiators in Biomedical Applications. *Polymers* **2020**, *12*, 1073. [CrossRef]
58. Photopolymerization Using Metal Oxide Semiconducting Nanoparticles for Epoxy-Based Coatings and Patterned Films. *ACS Appl. Nano Mater.* **2020**, *3*, 2875–2880. Available online: <https://pubs-acsc-org.lama.univ-amu.fr/doi/10.1021/acsnm.0c00147> (accessed on 24 April 2022). [CrossRef]
59. Breimer, M.A.; Yevgeny, G.; Sy, S.; Sadik, O.A. Incorporation of Metal Nanoparticles in Photopolymerized Organic Conducting Polymers: A Mechanistic Insight. *Nano Lett.* **2001**, *1*, 305–308. [CrossRef]
60. Guo, J.; Jian, J.; Wang, M.; Tomita, Y.; Cao, L.; Wang, D.; Zhang, X. Ag Nanoparticle-Enhanced Alkyl Radical Generation in Photopolymerization for Holographic Recording. *Nanophotonics* **2019**, *8*, 1795–1802. [CrossRef]
61. He, C.; Feng, Z.; Shan, S.; Wang, M.; Chen, X.; Zou, G. Highly Enantioselective Photo-Polymerization Enhanced by Chiral Nanoparticles and in Situ Photopatterning of Chirality. *Nat. Commun.* **2020**, *11*, 1188. [CrossRef] [PubMed]
62. Ibn-El-Ahrach, H.; Bachelot, R.; Lérondel, G.; Vial, A.; Grimault, A.-S.; Plain, J.; Royer, P.; Soppera, O. Controlling the Plasmon Resonance of Single Metal Nanoparticles by Near-Field Anisotropic Nanoscale Photopolymerization. *J. Microsc.* **2008**, *229*, 421–427. [CrossRef]
63. Ibn El Ahrach, H.; Bachelot, R.; Vial, A.; Lérondel, G.; Plain, J.; Royer, P.; Soppera, O. Spectral Degeneracy Breaking of the Plasmon Resonance of Single Metal Nanoparticles by Nanoscale Near-Field Photopolymerization. *Phys. Rev. Lett.* **2007**, *98*, 107402. [CrossRef] [PubMed]
64. Cai, X.; Anyaogu, K.C.; Neckers, D.C. Photopolymerization of Gold Nanoparticles: Size-Related Charge Separation and Emission. *J. Am. Chem. Soc.* **2007**, *129*, 11324–11325. [CrossRef] [PubMed]
65. Lv, J.; Lu, Y.; Wang, J.; Zhao, F.; Wang, Y.; He, H.; Wu, Y. Schiff Base-Type Copper(I) Complexes Exhibiting High Molar Extinction Coefficients: Synthesis, Characterization and DFT Studies. *J. Mol. Struct.* **2022**, *1249*, 131638. [CrossRef]
66. Kuang, D.; Ito, S.; Wenger, B.; Klein, C.; Moser, J.-E.; Humphry-Baker, R.; Zakeeruddin, S.M.; Grätzel, M. High Molar Extinction Coefficient Heteroleptic Ruthenium Complexes for Thin Film Dye-Sensitized Solar Cells. *J. Am. Chem. Soc.* **2006**, *128*, 4146–4154. [CrossRef]
67. Sciortino, G.; Maréchal, J.-D.; Fábíán, I.; Lihi, N.; Garrriba, E. Quantitative Prediction of Electronic Absorption Spectra of Copper(II)–Bioligand Systems: Validation and Applications. *J. Inorg. Biochem.* **2020**, *204*, 110953. [CrossRef]
68. Faggi, E.; Gavara, R.; Bolte, M.; Fajari, L.; Juliá, L.; Rodríguez, L.; Alfonso, I. Copper(II) Complexes of Macrocyclic and Open-Chain Pseudo-peptidic Ligands: Synthesis, Characterization and Interaction with Dicarboxylates. *Dalton Trans.* **2015**, *44*, 12700–12710. [CrossRef]
69. Iwamura, M.; Takeuchi, S.; Tahara, T. Ultrafast Excited-State Dynamics of Copper(I) Complexes. *Acc. Chem. Res.* **2015**, *48*, 782–791. [CrossRef]
70. Cuttell, D.G.; Kuang, S.-M.; Fanwick, P.E.; McMillin, D.R.; Walton, R.A. Simple Cu(I) Complexes with Unprecedented Excited-State Lifetimes. *J. Am. Chem. Soc.* **2002**, *124*, 6–7. [CrossRef] [PubMed]
71. Giereth, R.; Reim, I.; Frey, W.; Junge, H.; Tschierlei, S.; Karnahl, M. Remarkably Long-Lived Excited States of Copper Photosensitizers Containing an Extended π -System Based on an Anthracene Moiety. *Sustain. Energy Fuels* **2019**, *3*, 692–700. [CrossRef]
72. Egly, J.; Bissessar, D.; Achard, T.; Heinrich, B.; Steffanut, P.; Mauro, M.; Bellemin-Laponnaz, S. Copper(I) Complexes with Remotely Functionalized Phosphine Ligands: Synthesis, Structural Variety, Photophysics and Effect onto the Optical Properties. *Inorg. Chim. Acta* **2021**, *514*, 119971. [CrossRef]
73. Bergmann, L.; Hedley, G.J.; Baumann, T.; Bräse, S.; Samuel, I.D.W. Direct Observation of Intersystem Crossing in a Thermally Activated Delayed Fluorescence Copper Complex in the Solid State. *Sci. Adv.* **2016**, *2*, e1500889. [CrossRef]
74. Ochiai, H.; Miura, T.; Ikoma, T.; Minoura, M.; Nakano, H.; Matano, Y. Copper(II) Complexes of 10,20-Diaryl-5,15-Diazaporphyrin: Alternative Synthesis, Excited State Dynamics, and Substituent Effect on the $^1\text{O}_2$ -Generation Efficiency. *BCSJ* **2022**, *95*, 427–432. [CrossRef]

75. Fors, B.P.; Hawker, C.J. Control of a Living Radical Polymerization of Methacrylates by light. *Angew. Chem. Int. Ed.* **2012**, *51*, 8850. [[CrossRef](#)]
76. Ohtsuki, A.; Goto, A.; Kaji, H. Visible-Light-Induced Reversible Complexation Mediated Living Radical Polymerization of Methacrylates with Organic Catalysts. *Macromolecules* **2013**, *46*, 96. [[CrossRef](#)]
77. Cope, J.D.; Valle, H.U.; Hall, R.S.; Riley, K.M.; Goel, E.; Biswas, S.; Hendrich, M.P.; Wipf, D.O.; Stokes, S.L.; Emerson, J.P. Tuning the Copper(II)/Copper(I) Redox Potential for More Robust Copper-Catalyzed C–N Bond Forming Reactions. *Eur. J. Inorg. Chem.* **2020**, *2020*, 1278–1285. [[CrossRef](#)]
78. Tano, T.; Okubo, Y.; Kunishita, A.; Kubo, M.; Sugimoto, H.; Fujieda, N.; Ogura, T.; Itoh, S. Redox Properties of a Mononuclear Copper(II)-Superoxide Complex. *Inorg. Chem.* **2013**, *52*, 10431–10437. [[CrossRef](#)]
79. Asahi, M.; Yamazaki, S.; Itoh, S.; Ioroi, T. Electrochemical Reduction of Dioxygen by Copper Complexes with Pyridylalkylamine Ligands Dissolved in Aqueous Buffer Solution: The Relationship between Activity and Redox Potential. *Dalton Trans.* **2014**, *43*, 10705–10709. [[CrossRef](#)]
80. Nishikawa, M.; Kakizoe, D.; Saito, Y.; Ohishi, T.; Tsubomura, T. Redox Properties of Copper(I) Complex Bearing 4,7-Diphenyl-2,9-Dimethyl-1,10-Phenanthroline and 1,4-Bis(Diphenylphosphino)Butane Ligands and Effects of Light in the Presence of Chloroform. *BCSJ* **2017**, *90*, 286–288. [[CrossRef](#)]
81. Araya, L.M.; Vargas, J.A.; Costamagna, J.A. Ligand Influence on the Redox Properties of Some Copper(II) Complexes with Schiff Bases Derived from Bromosalicylaldehydes and Methyl or Chloro-Substituted Anilines. *Transit. Met. Chem.* **1986**, *11*, 312–316. [[CrossRef](#)]
82. Das, A.; Ren, Y.; Hessin, C.; Murr, M.D.-E. Copper Catalysis with Redox-Active Ligands. *Beilstein J. Org. Chem.* **2020**, *16*, 858–870. [[CrossRef](#)] [[PubMed](#)]
83. Yang, K.; Yang, X.; Deng, Z.; Zhang, L.; An, J. Copper Piperazine Complex with a High Diffusion Coefficient for Dye-Sensitized Solar Cells. *ACS Appl. Energy Mater.* **2021**, *4*, 14004–14013. [[CrossRef](#)]
84. Dragonetti, C.; Magni, M.; Colombo, A.; Fagnani, F.; Roberto, D.; Melchiorre, F.; Biagini, P.; Fantacci, S. Towards Efficient Sustainable Full-Copper Dye-Sensitized Solar Cells. *Dalton Trans.* **2019**, *48*, 9703–9711. [[CrossRef](#)]
85. Giordano, M.; Volpi, G.; Bonomo, M.; Mariani, P.; Garino, C.; Viscardi, G. Methoxy-Substituted Copper Complexes as Possible Redox Mediators in Dye-Sensitized Solar Cells. *New J. Chem.* **2021**, *45*, 15303–15311. [[CrossRef](#)]
86. Conradie, J. Polypyridyl Copper Complexes as Dye Sensitizer and Redox Mediator for Dye-Sensitized Solar Cells. *Electrochem. Commun.* **2022**, *134*, 107182. [[CrossRef](#)]
87. Magni, M.; Biagini, P.; Colombo, A.; Dragonetti, C.; Roberto, D.; Valore, A. Versatile Copper Complexes as a Convenient Springboard for Both Dyes and Redox Mediators in Dye Sensitized Solar Cells. *Coord. Chem. Rev.* **2016**, *322*, 69–93. [[CrossRef](#)]
88. Michaels, H.; Benesperi, I.; Edvinsson, T.; Muñoz-García, A.B.; Pavone, M.; Boschloo, G.; Freitag, M. Copper Complexes with Tetradentate Ligands for Enhanced Charge Transport in Dye-Sensitized Solar Cells. *Inorganics* **2018**, *6*, 53. [[CrossRef](#)]
89. Rui, H.; Shen, J.; Yu, Z.; Li, L.; Han, H.; Sun, L. Stable Dye-Sensitized Solar Cells Based on Copper(II/I) Redox Mediators Bearing a Pentadentate Ligand. *Angew. Chem. Int. Ed.* **2021**, *60*, 16156–16163. [[CrossRef](#)]
90. Dumur, F. Recent advances on visible light metal-based photocatalysts for polymerization under low light intensity. *Catalysts* **2019**, *9*, 736. [[CrossRef](#)]
91. Noirbent, G.; Dumur, F. Recent advances on copper complexes as visible light photoinitiators and (photo)redox initiators of polymerization. *Catalysts* **2020**, *10*, 953. [[CrossRef](#)]
92. Zivic, N.; Kuroishi, P.K.; Dumur, F.; Gígenes, D.; Dove, A.P.; Sardon, H. Recent advances and challenges in the design of organic photoacid and photobase generators for polymerizations. *Angew. Chem. Int. Ed.* **2019**, *58*, 10410–10422. [[CrossRef](#)] [[PubMed](#)]
93. Tehfe, M.-A.; Lalevé, J.; Dumur, F.; Telitel, S.; Gígenes, D.; Contal, E.; Bertin, D.; Fouassier, J.-P. Zinc-based metal complexes as new photocatalysts in polymerization initiating systems. *Eur. Polym. J.* **2013**, *49*, 1040–1049. [[CrossRef](#)]
94. Lalevé, J.; Telitel, S.; Xiao, P.; Lepeltier, M.; Dumur, F.; Morlet-Savary, F.; Gígenes, D.; Fouassier, J.-P. Metal and metal free photocatalysts: Mechanistic approach and application as photoinitiators of photopolymerization. *Beilstein J. Org. Chem.* **2014**, *10*, 863–876. [[CrossRef](#)]
95. Baralle, A.; Fensterbank, L.; Goddard, J.P.; Olivier, C. Aryl Radical Formation by Copper (I) Photocatalyzed Reduction of Diaryliodonium Salts. NMR Evidences for a Cu (II)/Cu (I) Mechanism. *Chem. Eur. J.* **2013**, *19*, 10809. [[CrossRef](#)]
96. Paria, S.; Reiser, O. Copper in Photocatalysis. *ChemCatChem* **2014**, *6*, 2477. [[CrossRef](#)]
97. Reiser, O. Shining Light on Copper: Unique Opportunities for Visible-Light-Catalyzed Atom Transfer Radical Addition Reactions and Related Processes. *Acc. Chem. Res.* **2016**, *49*, 1990. [[CrossRef](#)]
98. Hernandez-Perez, A.C.; Collins, S.K. Heteroleptic Cu-Based Sensitizers in Photoredox Catalysis. *Acc. Chem. Res.* **2016**, *49*, 1557. [[CrossRef](#)]
99. Hernandez-Perez, A.C.; Collins, S.K. A visible-light-mediated synthesis of carbazoles. *Angew. Chem. Int. Ed.* **2013**, *52*, 12696. [[CrossRef](#)]
100. Mau, A.; Dietlin, C.; Dumur, F.; Lalevé, J. Concomitant initiation of radical and cationic polymerisations using new copper complexes as photoinitiators: Synthesis and characterisation of acrylate/epoxy interpenetrated polymer networks. *Eur. Polym. J.* **2021**, *152*, 110457. [[CrossRef](#)]
101. Mau, A.; Noirbent, G.; Dietlin, C.; Graff, B.; Gígenes, D.; Dumur, F.; Lalevé, J. Panchromatic Copper Complexes for Visible Light Photopolymerization. *Photochem* **2021**, *1*, 167–189. [[CrossRef](#)]

102. Mokbel, H.; Anderson, D.; Plenderleith, R.; Dietlin, C.; Morlet-Savary, F.; Dumur, F.; Gigmes, D.; Fouassier, J.P.; Lalevée, J. Simultaneous initiation of radical and cationic polymerization reactions using the “G1” copper complex as photoredox catalyst: Applications of free radical/cationic hybrid photopolymerization in the composites and 3D printing fields. *Prog. Org. Coat.* **2019**, *132*, 50. [[CrossRef](#)]
103. AL Mousawi, A.; Kermagoret, A.; Versace, D.L.; Toufaily, J.; Hamieh, T.; Graff, B.; Dumur, F.; Gigmes, D.; Fouassier, J.P.; Lalevée, J. Copper photoredox catalysts for polymerization upon near UV or visible light: Structure/reactivity/efficiency relationships and use in LED projector 3D printing resins. *Polym. Chem.* **2017**, *8*, 568. [[CrossRef](#)]
104. Xiao, P.; Dumur, F.; Zhang, J.; Fouassier, J.-P.; Gigmes, D.; Lalevée, J. Copper complexes in radical photoinitiating systems: Applications to free radical and cationic polymerization under visible lights. *Macromolecules* **2014**, *47*, 3837–3844. [[CrossRef](#)]
105. Matsui, M.; Matsumoto, K.; Shibata, K.; Muramatsu, H. Synthesis and Characterization of 5-Cyano-6-Methyl-2,2'-Bipyridine Metal-Complex Dyes. *Dyes Pigments* **1992**, *18*, 47–55. [[CrossRef](#)]
106. Matsui, M.; Oji, A.; Hiramatsu, K.; Shibata, K.; Muramatsu, H. Synthesis and Characterization of Fluorescent 4,6-Disubstituted-3-Cyano-2-Methylpyridines. *J. Chem. Soc. Perkin Trans. 2* **1992**, *2*, 201–206. [[CrossRef](#)]
107. Knorn, M.; Rawner, T.; Czerwieńiec, R.; Reiser, O. [Copper(phenanthroline)(bisonitrile)]⁺-Complexes for the Visible-Light-Mediated Atom Transfer Radical Addition and Allylation Reactions. *ACS Catal.* **2015**, *5*, 5186–5193. [[CrossRef](#)]
108. Kaeser, A.; Mohankumar, M.; Mohanraj, J.; Monti, F.; Holler, M.; Cid, J.J.; Moudam, O.; Nierengarten, I.; Karmazin-Brelot, L.; Duhayon, C.; et al. Heteroleptic Copper(I) Complexes Prepared from Phenanthroline and Bis-Phosphine Ligands. *Inorg. Chem.* **2013**, *52*, 12140–12151. [[CrossRef](#)]
109. Wang, X.; Bai, X.; Su, D.; Zhang, Y.; Li, P.; Lu, S.; Gong, Y.; Zhang, W.; Tang, B. Simultaneous Fluorescence Imaging Reveals N-Methyl-d-aspartic Acid Receptor Dependent Zn²⁺/H⁺ Flux in the Brains of Mice with Depression. *Anal. Chem.* **2020**, *92*, 4101. [[CrossRef](#)]
110. Foresman, J.B.; Frisch, A. *Exploring Chemistry with Electronic Structure Methods*, 2nd ed.; Gaussian Inc.: Pittsburgh, PA, USA, 1996.
111. Frisch, M.J.; Trucks, G.W.; Schlegel, H.B.; Scuseria, G.E.; Robb, M.A.; Cheeseman, J.R.; Zakrzewski, V.G.; Montgomery, J.A.; Stratmann, J.R.E.; Burant, J.C.; et al. *Gaussian 03, Revision B-2*; Gaussian Inc.: Pittsburgh, PA, USA, 2003.
112. Al Mousawi, A.; Dumur, F.; Garra, P.; Toufaily, J.; Hamieh, T.; Goubard, F.; Bui, T.T.; Graff, B.; Gigmes, D.; Fouassier, J.P.; et al. Azahelicenes as visible light photoinitiators for cationic and radical polymerization: Preparation of photoluminescent polymers and use in high performance LED projector 3D printing resins. *J. Polym. Sci. A Polym. Chem.* **2017**, *55*, 1189. [[CrossRef](#)]
113. Dong, F.; Jian, C.; Zhenghao, F.; Kai, G.; Zuliang, L. Synthesis of Chalcones via Claisen–Schmidt Condensation Reaction Catalyzed by Acyclic Acidic Ionic Liquids. *Catal. Commun.* **2008**, *9*, 1924–1927. [[CrossRef](#)]
114. Rafiee, E.; Rahimi, F. A Green Approach to the Synthesis of Chalcones via Claisen–Schmidt Condensation Reaction Using Cesium Salts of 12-Tungstophosphoric Acid as a Reusable Nanocatalyst. *Monatsh. Chem.* **2013**, *144*, 361–367. [[CrossRef](#)]
115. Mousavi, S.R. Claisen–Schmidt Condensation: Synthesis of (1S,6R)/(1R,6S)-2-Oxo-N,4,6-Triaryl-cyclohex-3-Enecarboxamide Derivatives with Different Substituents in H₂O/EtOH. *Chirality* **2016**, *28*, 728–736. [[CrossRef](#)]
116. Kumar, D.; Suresh; Sandhu, J.S. An Efficient Green Protocol for the Synthesis of Chalcones by a Claisen–Schmidt Reaction Using Bismuth(III)Chloride as a Catalyst under Solvent-Free Condition. *Green Chem. Lett. Rev.* **2010**, *3*, 283–286. [[CrossRef](#)]
117. Ekanayake, U.G.M.; Weerathunga, H.; Weerasinghe, J.; Waclawik, E.R.; Sun, Z.; MacLeod, J.M.; O’Mullane, A.P.; Ostrikov, K. (Ken) Sustainable Claisen–Schmidt Chalcone Synthesis Catalysed by Plasma-Recovered MgO Nanosheets from Seawater. *Sustain. Mater. Technol.* **2022**, *32*, e00394. [[CrossRef](#)]
118. Parekh, A.K.; Desai, K.K. Synthesis and Antibacterial Activity of Chalcones and Pyrimidine-2-Ones. *E-J. Chem.* **1900**, *2*, 134830. [[CrossRef](#)]
119. Jesus, A.R.; Marques, A.P.; Rauter, A.P. An Easy Approach to Dihydrochalcones via Chalcone in Situ Hydrogenation. *Pure Appl. Chem.* **2016**, *88*, 349–361. [[CrossRef](#)]
120. Julakanti, S.R.; Patel, M.; Ponneri, V. Highly Efficient Synthesis of Chalcones from Poly Carbonyl Aromatic Compounds Using BF₃–Et₂O via a Regioselective Condensation Reaction. *Chem. Pharm. Bull.* **2016**, *64*, 570–576. [[CrossRef](#)]
121. Winter, C.; Caetano, J.N.; Araújo, A.B.C.; Chaves, A.R.; Ostroski, I.C.; Vaz, B.G.; Pérez, C.N.; Alonso, C.G. Activated Carbons for Chalcone Production: Claisen–Schmidt Condensation Reaction. *Chem. Eng. J.* **2016**, *303*, 604–610. [[CrossRef](#)]
122. Qian, H.; Liu, D.; Lv, C. Synthesis of Chalcones via Claisen–Schmidt Reaction Catalyzed by Sulfonic Acid-Functional Ionic Liquids. *Ind. Eng. Chem. Res.* **2011**, *50*, 1146–1149. [[CrossRef](#)]
123. Calvino, V.; Picallo, M.; López-Peinado, A.J.; Martín-Aranda, R.M.; Durán-Valle, C.J. Ultrasound Accelerated Claisen–Schmidt Condensation: A Green Route to Chalcones. *Appl. Surf. Sci.* **2006**, *252*, 6071–6074. [[CrossRef](#)]
124. Li, J.-T.; Yang, W.-Z.; Wang, S.-X.; Li, S.-H.; Li, T.-S. Improved Synthesis of Chalcones under Ultrasound Irradiation. *Ultrason. Sonochem.* **2002**, *9*, 237–239. [[CrossRef](#)]
125. Bui, T.H.; Nguyen, N.T.; Dang, P.H.; Nguyen, H.X.; Nguyen, M.T.T. Design and Synthesis of Chalcone Derivatives as Potential Non-Purine Xanthine Oxidase Inhibitors. *SpringerPlus* **2016**, *5*, 1789. [[CrossRef](#)] [[PubMed](#)]